

Coordination versatility of tridentate pyridyl aroylhydrazones towards iron: tracking down the elusive aroylhydrazono-based ferric spin-crossover molecular materials†Musa S. Shongwe,^{*a} Sumaiya H. Al-Rahbi,^a Mariam A. Al-Azani,^a Abdulaziz A. Al-Muharbi,^a Faizah Al-Mjeni,^a Dariusz Matoga,^b Abbasher Gismelseed,^c Imaddin A. Al-Omari,^c Ali Yousif,^c Harry Adams,^d Michael J. Morris^d and Masahiro Mikuriya^e

Received 25th July 2011, Accepted 10th November 2011

DOI: 10.1039/c1dt11407g

The two potentially tridentate and monoprotic Schiff bases acetylpyridine benzoylhydrazone (HL¹) and acetylpyridine 4-*tert*-butylbenzoylhydrazone (HL²) demonstrate remarkable coordination versatility towards iron on account of their propensity to undergo tautomeric transformations as imposed by the metal centre. Each of the pyridyl aroylhydrazone ligands complexes with the ferrous or ferric ion under strictly controlled reaction conditions to afford three six-coordinate mononuclear compounds [Fe^{II}(HL)₂](ClO₄)₂, [Fe^{II}L₂] and [Fe^{III}L₂]ClO₄ (HL = HL¹ or HL²) displaying distinct colours congruent with their intense CT visible absorptions. The synthetic manoeuvres rely crucially on the stoichiometry of the reactants, the basicities of the reaction mixtures and the choice of solvent. Electrochemically, each of these iron compounds exhibits a reversible metal-centred redox process. By all appearances, [Fe^{III}(L¹)₂]ClO₄ is one of only two examples of a crystallographically elucidated iron(III) bis-chelate compound of a pyridyl aroylhydrazone. Several pertinent physical measurements have established that each of the Schiff bases stabilises multiple spin states of iron; the enolate form of these ligands exhibits greater field strength than does the corresponding neutral keto tautomer. To the best of our knowledge, [Fe^{III}(L¹)₂]ClO₄ and [Fe^{III}(L²)₂]ClO₄ are the first examples of *ferric* spin crossovers of *aroylhydrazones*. Whereas in the former the spin crossover (SCO) is an intricate gradual process, in the latter the ⁶A₁ ↔ ²T₂ transition curve is sigmoidal with T_{1/2} ~280 K and the SCO is virtually complete. As regards [Fe^{III}(L¹)₂]ClO₄, Mössbauer and EPR spectroscopic techniques have revealed remarkable dependence of the spin transition on sample type and extent of solvation. In frozen MeOH solution at liquid nitrogen temperature, both iron(III) compounds exist wholly in the doublet ground state.

Introduction

The high efficacy, selectivity and specificity of the coordination of aroylhydrazones towards iron has rendered these Schiff bases prime candidates in the development of iron chelators for the treatment of iron overload in humans arising from β-thalassemia (a genetic disease) and hemochromatosis (chronic iron poisoning).

In recent times, there has been a concerted research endeavour to explore a diverse range of aroylhydrazones¹ and other related Schiff bases, such as thiosemicarbazones,^{1a,2} as potential iron-chelating drugs prompted by the overriding need for possible replacements for, or alternatives to, desferrioxamine (DFO),³ the siderophore currently enjoying world-wide clinical use in iron chelation therapy. For decades, DFO has been the sole clinically approved drug for the treatment of iron-overload disorders; however, its major drawback is that it is orally inactive, necessitating frequent and lengthy subcutaneous infusions, thereby causing poor compliance by patients. The iron chelators deferiprone,³ deferitricin⁴ and deferasirox,⁵ which have emerged recently, exhibit different degrees of oral effectiveness and are at different developmental stages, but all seem to be credible alternatives to DFO. As for aroylhydrazones,¹ studies have shown that these chelating agents are adequately lipophilic to permeate cell membranes and readily access intracellular iron. The potential biological applications of these ligands extend to prevention of malaria and treatment of several types of aggressive cancer.^{1,2}

^aDepartment of Chemistry, College of Science, Sultan Qaboos University, PO Box 36, Al-Khod 123, Muscat, Sultanate of Oman. E-mail: musa@squ.edu.om; Tel: +968 92163719

^bFaculty of Chemistry, Jagiellonian University, Ingardena 3, 30-060, Kraków, Poland

^cDepartment of Physics, College of Science, Sultan Qaboos University, PO Box 36, Al-Khod 123, Muscat, Sultanate of Oman

^dDepartment of Chemistry, University of Sheffield, Sheffield, UK, S3 7HF

^eDepartment of Chemistry, School of Science and Technology, Kwansai Gakuin University, 2-1 Gakuen, Sanda, 669-1337, Japan

† Electronic supplementary information (ESI) available. CCDC reference numbers 836952. For ESI and crystallographic data in CIF or other electronic format see DOI: 10.1039/c1dt11407g

From a structural perspective, aroylhydrazones are fascinating on account of their coordination versatility towards a diverse range of metals, particularly transition metals.⁶ To form complexes, these polydentate ligands satisfy charge-neutrality requirements and meet stereochemical demands of metal ions by facile tautomerisation followed by deprotonation.^{6,7} A given mixed-donor aroylhydrazone is capable of exhibiting several coordination modes and denticities with more than one combination of the donor atoms.⁸ As regards the coordination chemistry of iron with aroylhydrazones, the literature has revealed preference of phenolate- and naphtholate-possessing aroylhydrazones for the ferric state.⁶ On the other hand, the corresponding pyridyl derivatives tend to stabilise the ferrous state^{1c-f} under ambient conditions. However, pyridyl diaroylhydrazines and pyridyl diacylhydrazines, which are diamines rather than imines (Schiff bases), form iron(III) complexes.⁹ In this work, we demonstrate that the trivalent state of iron can be readily accessed for the pyridyl aroylhydrazones by a rather unconventional reaction stoichiometry of HL and Fe^{III} under basic conditions.

As the past decade drew to a close, the literature witnessed the emergence of crystallographically elucidated iron(II)-based pyridyl aroylhydrazone spin-crossover complexes.¹⁰ Hydrazones, whatever the type, are extremely rare in the realm of iron spin crossovers. The only structurally characterised hydrazone-based iron(III) spin-crossover complex {[Fe(mph)₂](ClO₄)·0.5MeOH·0.5H₂O}₂ [Hmph = 2-methoxy-6-(pyridyl-2-ylhydrazonomethyl)phenol]¹¹ possesses phenolate and pyridyl moieties (*i.e.* a different donor set from that provided by an aroylhydrazone). Herein we present the single-crystal X-ray structure of the iron(III) pyridyl aroylhydrazone complex [Fe^{III}(L¹)₂](ClO₄). The only other structurally characterised ferric complex of this type is the fortuitous alkoxy compound of Gao *et al.*¹⁰ whose synthesis entailed modification of the aroylhydrazone by substituting the proton of the aldimine (azomethine) moiety with the ethoxy group from the solvent. Our synthetic strategy differs from that of Gao *et al.*¹⁰ in that it leaves the identity of the ligand intact.

Whereas the development of the spin-crossover phenomenon in iron(II) complexes is occurring at a phenomenal pace, there is a mere trickle of iron(III) spin-crossover complexes in the literature. Spin crossovers are currently being pursued with much vigour due to insatiable curiosity about this phenomenon and the growing realisation of the potential technological applications of such magnetically switchable bistable materials in molecular electronics.¹² In the case of six-coordinate iron complexes, the ligand field strength and coordination sphere can be modulated to support the following types of spin transition: $S = 2 \leftrightarrow S = 0$ for Fe^{II};^{12a-d,f-j} and $S = 5/2 \leftrightarrow S = 1/2$,^{11,12e,g,13} $S = 5/2 \leftrightarrow S = 3/2$ ¹⁴ and $S = 3/2 \leftrightarrow 1/2$ ¹⁵ for Fe^{III}. The vast majority of iron(II) spin crossovers have the donor set [N₆];^{12a-d,f-h,j} a mere handful have the donor set [N₄O₂].^{12i,16} Conversely, iron(III) spin crossovers with the [Fe^{III}N₄O₂]^{11,12e,g,m,13} core by far outnumber those with all-*N*-donor coordination spheres.¹⁷ Spin transition curves have revealed various types of SCO features such as abrupt, gradual, two-step, complete, incomplete and hysteretic spin transformations along with several combinations thereof.¹⁰⁻¹⁷ Abrupt, two-step and hysteretic spin transitions tend to reflect cooperative intermolecular interactions in the solid state. Two-step transitions can be two-sided^{11,13a,16a,d,18} (with two crystallographically distinct paramagnetic centres undergoing independent spin

transitions), one-sided¹⁹ or symmetry-breaking²⁰ (involving at least two different crystallographic phases including an intermediate phase comprising distinct spin states); examples of each of these are few and far between.

This work was undertaken with the following three-pronged motivation: (1) to demonstrate the remarkable coordination versatility of pyridyl aroylhydrazones towards iron by merely varying and strictly controlling the reaction conditions; (2) to conduct targeted syntheses and isolation of the first examples of ferric bis-chelate complexes of pyridyl aroylhydrazones and provide crystallographic elucidation of their structures; and (3) to fine-tune the ligand-field strength in a structural design that promotes iron(III)-based spin crossover. The pyridyl aroylhydrazones employed in this work are displayed in Scheme 1 together with their designations.

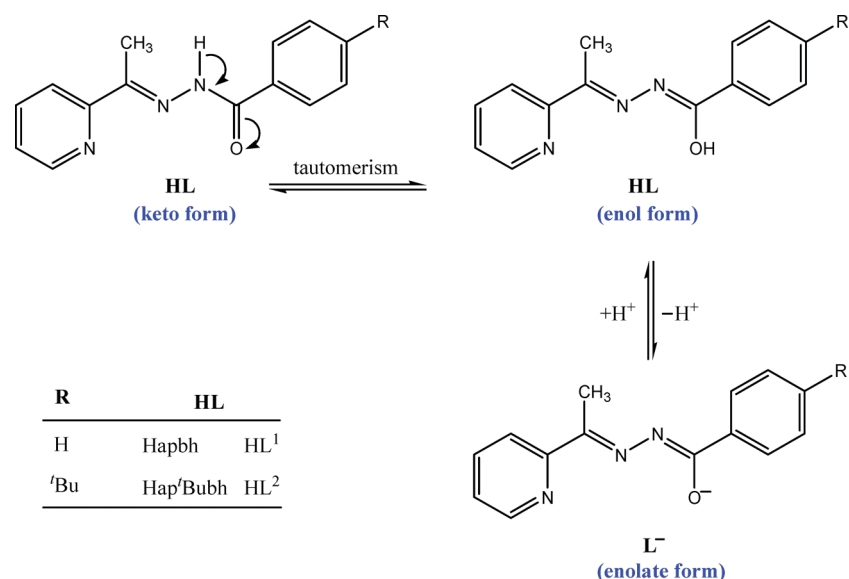
Results and discussion

Syntheses and identification of ligands and iron complexes

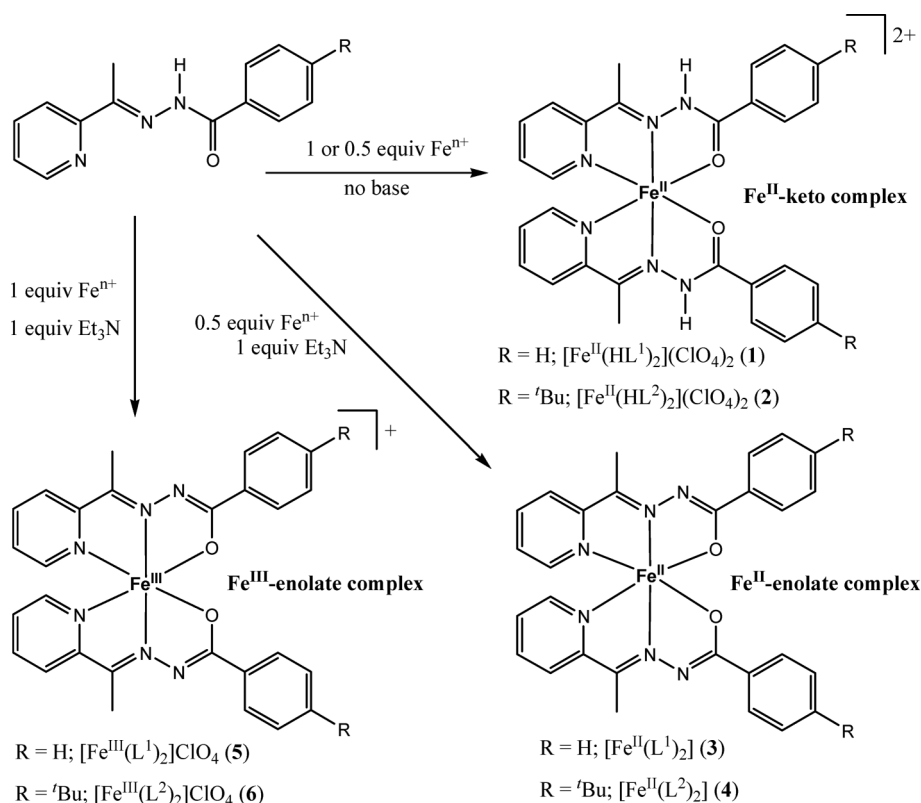
The Schiff bases 2-acetylpyridine benzoylhydrazone (Hapbh = HL¹)^a and 2-acetylpyridine 4-*tert*-butylbenzoylhydrazone (Hap'Bubh = HL²) were synthesised straightforwardly by condensation reactions between 2-acetylpyridine (a pyridyl ketone) and the appropriate aroylhydrazide (a primary amine) in equimolar amounts in refluxing EtOH. The products were obtained in high yields (>80%) with HL¹ isolated as shiny long colourless needles and HL² as a lustrous white microcrystalline material. The chemical compositions of these aroylhydrazones were ascertained by microanalyses (C, H and N) and the molar masses were verified by the molecular peaks in the EI mass spectra: $m/z = 239$ (HL¹) and 295 (HL²).

That these ligands are Schiff bases is proven by the presence of an absorption band at 1617 and 1610 cm⁻¹ in the IR spectra of HL¹ and HL², respectively, ascribable to the characteristic azomethine (C=N) bond. Vibrational spectroscopy shows that these pyridyl aroylhydrazones adopt the keto tautomeric form (Scheme 1) in the solid state with the amide functional group identifiable by its typical $\nu(\text{N-H})$ and $\nu(\text{C=O})$ absorptions (3176 and 1653 cm⁻¹, respectively, for HL¹; 3254 and 1666 cm⁻¹, respectively, for HL²). The ketimine methyl group stands out in the ¹H NMR spectra of these ligands in CDCl₃: δ 2.49 for HL¹ and δ 2.48 for HL² (Fig. S1 and S2, respectively, ESI†). More importantly, ¹H NMR spectroscopy revealed that the ligand keto structural identity is retained in solution as evidenced by the broad resonances at δ 9.29 (HL¹) and δ 9.12 (HL²), associated with the amide-NH portion. Incidentally, these signals are solvent-dependent with more downfield chemical shifts in DMSO-*d*₆ (δ 10.87 for HL¹ and δ 10.77 for HL²). The IR and ¹H NMR spectra of HL² differ conspicuously from the corresponding ones of HL¹ by the characteristic three-band absorption pattern (2966, 2902 and 2868 cm⁻¹) and intense singlet (δ 1.36), respectively, attributable to the *tert*-butyl substituent group in HL².

By exploiting the tendency of aroylhydrazones to undergo metal- or base-assisted tautomeric transformations with much ease, a synthetic strategy to generate more than one iron complex from each pyridyl aroylhydrazone was devised. Reactions of each of the ligands (HL) were carried out meticulously under strictly controlled conditions to afford three compounds with the general



Scheme 1 Tautomeric transformation of pyridyl aroylhydrazones.



Scheme 2 Strategic syntheses of three iron compounds from each of the pyridyl aroylhydrazones HL¹ and HL². All reactions were performed under aerobic conditions.

formulae [Fe^{II}(HL)₂](ClO₄)₂, [Fe^{II}L₂] and [Fe^{III}L₂](ClO₄) (Scheme 2): specifically, [Fe^{II}(HL¹)₂](ClO₄)₂ (**1**)²¹ (purple-violet crystals), [Fe^{II}(L²)₂] (**3**)^{1f,10a} (dark green crystals) and [Fe^{III}(L¹)₂](ClO₄) (**5**) (black crystals) from HL¹ and [Fe^{II}(HL²)₂](ClO₄)₂ (**2**) (purple powder), [Fe^{II}(L²)₂] (**4**) (dark green crystals) and [Fe^{III}(L²)₂](ClO₄) (**6**) (olive crystalline sheets) from HL².

The ionic iron(II) compounds **1** and **2** were synthesised by the reaction of Fe(ClO₄)₂·6H₂O or Fe(ClO₄)₃·xH₂O with two molar

equivalents (or an equal amount) of the appropriate aroylhydrazone ligand (*i.e.*, either an Feⁿ⁺:HL molar ratio of 1:1 or 1:2) in MeOH or a mixture of MeOH and EtOH (50% v/v) in air under reflux over a period of 15 min; crucially, the base (triethylamine) must be excluded from this reaction. Interestingly, in the case of HL¹, when the iron salt was Fe(ClO₄)₃·xH₂O, the product was obtained overnight as the dihydrate [Fe^{II}(HL¹)₂](ClO₄)₂·2H₂O, but when the salt was Fe(ClO₄)₂·2H₂O the product was obtained

immediately in the anhydrous form (see Experimental). The molecular (non-ionic) ferrous compounds **3** and **4** were produced by an analogous synthetic procedure but adhering strictly to an $\text{Fe}^{n+}:\text{HL}$ stoichiometric ratio of 1:2 in the presence of triethylamine as a base. Evidently, the tautomerism of the pyridyl aroylhydrazones to form these two complexes is base-driven. The generation of the ionic ferric compounds **5** and **6** required strictly an $\text{Fe}^{n+}:\text{HL}$ molar ratio of 1:1 and the presence of a base; clearly, in this reaction the Fe^{n+} is in excess. The solvation of the product depends on the method of synthesis: the template reaction afforded the hydrated product $[\text{Fe}^{\text{III}}(\text{L}^1)_2]\text{ClO}_4 \cdot 2\text{H}_2\text{O}$ whereas the stepwise reaction yielded the product with a MeOH solvent of crystallisation $[\text{Fe}^{\text{III}}(\text{L}^1)_2]\text{ClO}_4 \cdot \text{MeOH}$. On isolation from the mother liquor, these two solvated compounds lose their solvents of crystallisation gradually, finally giving the non-solvated compound $[\text{Fe}^{\text{III}}(\text{L}^1)_2]\text{ClO}_4$. In these three synthetic routes (Scheme 2), the pyridyl aroylhydrazones support both the spontaneous oxidation of Fe^{II} (salt) to Fe^{III} (complex) and the spontaneous reduction of Fe^{III} (salt) to Fe^{II} (complex) depending on the reaction conditions.

The iron(II) compounds $[\text{Fe}^{\text{II}}(\text{HL}^1)_2](\text{ClO}_4)_2$ ²¹ and $[\text{Fe}^{\text{II}}(\text{L}^1)_2]$ ^{16,10a} have been reported previously, but not in a systematic synthetic study as in this work whereby one of the goals is to highlight the coordination versatility of pyridyl aroylhydrazones. However, we note that the use of an inert atmosphere, strictly a ferrous salt and large excess of a base as well as prolonged reaction times as reported in the literature for the syntheses of $[\text{Fe}^{\text{II}}(\text{L}^1)_2]$ ^{16,10a} and its congeners^{1c,6,10} are unnecessary: the crucial condition is strict adherence to stoichiometric amounts of the reactants and the base. As for the iron(III) compounds **5** and **6**, to the best of our knowledge, this is the first time they have ever been *isolated* (with the ligand remaining intact) and fully characterised, even though their analogues have been electrochemically generated and proven to exist by EPR spectroscopy.^{1c,d}

The elusiveness of these iron(III) pyridyl aroylhydrazono compounds probably stems in part from the unconventional synthetic requirement of an $\text{HL}:\text{Fe}^{n+}$ molar ratio of 1:1 to form the bis-chelate complexes. The colour differences amongst the three iron compounds $[\text{Fe}^{\text{II}}(\text{HL})_2](\text{ClO}_4)_2$, $[\text{Fe}^{\text{II}}\text{L}_2]$ and $[\text{Fe}^{\text{III}}\text{L}_2]\text{ClO}_4$ ($\text{HL} = \text{HL}^1$ or HL^2) from the same ligand are appreciated in solution. In MeOH solution, $[\text{Fe}^{\text{II}}\text{L}_2]$ and $[\text{Fe}^{\text{III}}\text{L}_2]\text{ClO}_4$ are dark green and olive, respectively. Unfortunately, interactions of the compounds $[\text{Fe}^{\text{II}}(\text{HL})_2](\text{ClO}_4)_2$ with MeOH under aerobic conditions readily convert these iron(II) compounds to the corresponding iron(III) compounds $[\text{Fe}^{\text{III}}\text{L}_2]\text{ClO}_4$ as evidenced by the colour changes of **1** (purple-violet) and **2** (purple) to olive on dissolution in this solvent. However, **1** is stable in MeCN, giving a purple-tinged pink solution. In contrast, the *tert*-substituted complex **2** is not stable in any common solvent in coordination chemistry (e.g. MeOH, EtOH, Me_2CO , MeCN, DMSO, DMF, CHCl_3 and CH_2Cl_2) with respect to aerial oxidation.

The elemental compositions and chemical formulations of $[\text{Fe}^{\text{II}}(\text{HL})_2](\text{ClO}_4)_2$, $[\text{Fe}^{\text{II}}\text{L}_2]$ and $[\text{Fe}^{\text{III}}\text{L}_2]\text{ClO}_4$ were ascertained by microanalyses (C, H & N) and FAB mass spectrometry; subsequently, these were corroborated by molar conductivity measurements²² and IR spectroscopy. The FAB mass spectra of $[\text{Fe}^{\text{II}}\text{L}_2]$ and $[\text{Fe}^{\text{III}}\text{L}_2]\text{ClO}_4$ in the positive mode are identical: the molecular peaks of the complex cations “ $[\text{Fe}^{\text{II}}(\text{L}^1)_2]^+$ ”/“ $[\text{Fe}^{\text{III}}(\text{L}^1)_2]^+$ ” occur at $m/z = 532$ whereas those of “ $[\text{Fe}^{\text{II}}(\text{L}^2)_2]^+$ ”/“ $[\text{Fe}^{\text{III}}(\text{L}^2)_2]^+$ ”

appear at $m/z = 644$. To illustrate the fragmentation pattern of each complex cation, the FAB mass spectrum of $[\text{Fe}^{\text{III}}(\text{L}^1)_2]\text{ClO}_4$ (**5**) is presented in Fig. S3, ESI.† Clearly, the aroylhydrazone ligands dissociate in two stages: the peak at $m/z = 294$ is indicative of a loss of ligand from $[\text{Fe}^{\text{III}}(\text{L}^1)_2]^+$ to give “ $[\text{Fe}^{\text{III}}(\text{L}^1)]^+$ ” and the second loss of ligand is shown by the peak at $m/z = 237$. A similar pattern is observed in the spectra of the other bis-chelate complexes. Conductivity measurements²² demonstrated unequivocally the differences amongst the compounds $[\text{Fe}^{\text{II}}(\text{HL})_2](\text{ClO}_4)_2$, $[\text{Fe}^{\text{II}}\text{L}_2]$ and $[\text{Fe}^{\text{III}}\text{L}_2]\text{ClO}_4$. The purple compound $[\text{Fe}^{\text{II}}(\text{HL}^1)_2](\text{ClO}_4)_2$ (**1**) has molar conductance of $260 \text{ S cm}^2 \text{ mol}^{-1}$ in MeCN consistent with a 2:1 electrolyte type.¹⁷ On the other hand, the dark green complexes $[\text{Fe}^{\text{II}}(\text{L}^1)_2]$ (**3**) and $[\text{Fe}^{\text{II}}(\text{L}^2)_2]$ (**4**) are molecular, rather than ionic, as their solutions in methanol are non-electrolytes ($\Lambda_{\text{M}} = 0 \text{ S cm}^2 \text{ mol}^{-1}$). The olive ferric compounds $[\text{Fe}^{\text{III}}(\text{L}^1)_2]\text{ClO}_4$ (**5**) and $[\text{Fe}^{\text{III}}(\text{L}^2)_2]\text{ClO}_4$ (**6**) are 1:1 electrolytes in methanol ($\Lambda_{\text{M}} \sim 80$ and $85 \text{ S cm}^2 \text{ mol}^{-1}$, respectively). Thus it is clear that each pyridyl aroylhydrazone undergoes metal- and base-assisted tautomerisation.

The most obvious feature in the IR spectra of the iron compounds is the presence or absence of the absorptions of the perchlorate counter ion [$\nu(\text{ClO}_4^-)$: $\sim 1100\text{--}1080 \text{ cm}^{-1}$ (very strong), $\sim 625 \text{ cm}^{-1}$ (medium intensity)]. In keeping with the results of the conductivity measurements, the IR spectra of the ionic iron(II) compounds **1** and **2** as well as the ionic iron(III) compounds **5** and **6** confirmed the presence of the perchlorate ion, with noticeably more intense absorption bands for the ferrous compounds possessing two such ions each. On the other hand, as expected, the molecular (non-ionic) iron(II) complexes **3** and **4** do not exhibit $\nu(\text{ClO}_4^-)$ absorptions in their spectra.

That the pyridyl aroylhydrazone ligands in these complexes are Schiff bases is indicated by the vibrational bands of the imine $\text{C}=\text{N}$ bond in the range $1598\text{--}1636 \text{ cm}^{-1}$. The ligands in the complexes $[\text{Fe}^{\text{II}}\text{L}_2]$ and $[\text{Fe}^{\text{III}}\text{L}_2]\text{ClO}_4$ underwent metal- and base-assisted tautomerism whereby the amide functional group was converted to the enolate form. The keto $\text{C}=\text{O}$ double bond converted to the enolate $\text{C}-\text{O}^-$ single bond and the amide $\text{C}-\text{N}$ single bond became a double bond. This tautomeric transformation is indicated conspicuously by the disappearance of the characteristic $\text{N}-\text{H}$ and $\text{C}=\text{O}$ vibrational absorptions and the appearance of new intense absorptions in the ranges $\sim 1350\text{--}1490 \text{ cm}^{-1}$ and $\sim 1520\text{--}1600 \text{ cm}^{-1}$ for the enolate backbone. Contrariwise, in the formation of the complexes $[\text{Fe}(\text{HL})_2](\text{ClO}_4)_2$ the keto tautomer of the ligand remains intact. While it is not possible to identify the absorption bands of the coordinated amide $\text{C}=\text{O}$ groups unequivocally in the IR spectra of these keto complexes, the amide $-\text{NH}$ groups stand out prominently at 3450 and 3250 cm^{-1} for the complexes $[\text{Fe}(\text{HL}^1)](\text{ClO}_4)_2$ and $[\text{Fe}(\text{HL}^2)](\text{ClO}_4)_2$, respectively. Other ligand features of interest include the *tert*-butyl substituent groups, which exhibit a characteristic three-band pattern of absorptions in the range $2860\text{--}2970 \text{ cm}^{-1}$.

Single-crystal X-ray analysis of $[\text{Fe}^{\text{III}}(\text{L}^1)_2]\text{ClO}_4$ (**5**)

Rectangular-shaped black blocks of $[\text{Fe}^{\text{III}}(\text{L}^1)_2]\text{ClO}_4$ (**5**) were obtained from a solution of this compound in EtOH/MeOH (1:1, v/v) by slow evaporation over a period of three days at room temperature. The crystallographic data were collected on a crystal with the dimensions $0.46 \text{ mm} \times 0.22 \text{ mm} \times 0.10 \text{ mm}$ at

Table 1 Crystal data and structure refinement for [Fe^{III}(L¹)₂]ClO₄ (**5**)

Empirical formula	C ₂₈ H ₃₄ N ₆ O ₆ ClFe
Molar mass	631.83 g mol ⁻¹
Temperature	100(2) K
Wavelength	0.71073 Å
Crystal system	Triclinic
Space group	<i>P</i> $\bar{1}$
Unit cell dimensions	<i>a</i> = 11.6635(4) Å <i>b</i> = 14.7148(5) Å <i>c</i> = 17.9725(9) Å α = 71.4020(10) $^\circ$ β = 88.945(2) $^\circ$ γ = 87.4680(10) $^\circ$
Volume	2920.6(2) Å ³
Z	4
Density (calculated)	1.437 Mg m ⁻³
Absorption coefficient	0.660 mm ⁻¹
<i>F</i> (000)	1300
Crystal dimensions	0.46 × 0.22 × 0.10 mm ³
Theta range for data collection	1.20–31.09 $^\circ$
Reflections collected	41 361
Independent reflections	16294 [<i>R</i> _{int} = 0.0394]
Completeness to theta = 25.00 $^\circ$	99.3%
Max. and min. transmission	0.9370 and 0.7512
Data/restraints/parameters	16 294/26/747
Goodness-of-fit on <i>F</i> ²	1.012
Final <i>R</i> indices [<i>I</i> > 2σ(<i>I</i>)]	<i>R</i> ₁ = 0.0896, <i>wR</i> ₂ = 0.2702
<i>R</i> indices (all data)	<i>R</i> ₁ = 0.1417, <i>wR</i> ₂ = 0.3022
Largest diff. peak and hole	2.910 and -2.579 e.Å ⁻³

100 K. This iron(III) compound crystallised in the triclinic system with the space group *P* $\bar{1}$. Interestingly, in contrast, the corresponding iron(II) analogue, [Fe^{II}(L¹)₂] (**3**),^{10a} crystallised in the monoclinic space group *Cc* even though it comprises the same ligand as that in **5**, *i.e.* (L¹)⁻. Crystal data as well as parameters for structure solution and refinement for **5** are presented in Table 1.

The X-ray structure of **5** is represented by the ORTEP diagram in Fig. 1 while selected bond distances and angles are listed in Table 2. N.B. A solvent molecule of crystallisation that proved difficult to refine was eliminated by applying the 'Squeeze' function in PLATON.²³ The crystal was not of high quality, but the best from relentless crystallisation attempts spanning three years. It is noteworthy that loss of the solvate has an adverse effect on the ability of the crystals to diffract.

To the best of our knowledge, **5** is one of only two examples of a crystallographically elucidated iron(III) compound of this kind possessing a pyridyl aroylhydrazone. (The other example is [Fe(L-OEt)₂]ClO₄·EtOH·H₂O,^{10a} but in the formation of this compound the identity of the aroylhydrazone was modified by a side substitution reaction). The crystallographic asymmetric unit of **5** comprises two discrete complex cations, which are similar but not identical, and two perchlorate counter anions. One of the perchlorate ions is severely disordered, raising the value of the *R*-factor to 8.96%. Each of the complex cations consists of two aroylhydrazone ligands oriented virtually orthogonally to each other and coordinating to the iron(III) ion in a tridentate fashion to afford a six-coordinate geometry by employing the following donor atoms: a pyridyl nitrogen, an imine nitrogen and an enolate oxygen. The chelate donor atoms adopt a meridional coordination mode; thus the two imine nitrogen atoms occupy *trans* positions whereas each of the two pairs of pyridyl nitrogen atoms and enolate oxygen atoms takes adjacent positions to give a *trans,cis,cis*-coordination arrangement consistent with the rigidity and planarity of the Schiff-base ligand.

Table 2 Selected bond distances (Å) and angles (°) for [Fe^{III}(L¹)₂]ClO₄ (**5**)

Complex cation A		Complex cation B	
Fe(2)–N(1A)	1.894(4)	Fe(1)–N(1B)	1.876(4)
Fe(2)–N(3A)	1.972(4)	Fe(1)–N(3B)	1.952(3)
Fe(2)–N(5A)	1.884(3)	Fe(1)–N(5B)	1.881(4)
Fe(2)–N(6A)	1.955(4)	Fe(1)–N(6B)	1.944(4)
Fe(2)–O(1A)	1.894(3)	Fe(1)–O(1B)	1.905(3)
Fe(2)–O(2A)	1.910(3)	Fe(1)–O(2B)	1.911(3)
C(13A)–N(1A)	1.307(5)	C(13B)–N(1B)	1.310(5)
C(22A)–N(5A)	1.313(5)	C(22B)–N(5B)	1.300(5)
N(1A)–N(2A)	1.360(5)	N(1B)–N(2B)	1.367(5)
N(4A)–N(5A)	1.371(5)	N(4B)–N(5B)	1.373(5)
N(2A)–C(1A)	1.337(5)	N(2B)–C(1B)	1.318(5)
N(4A)–C(15A)	1.331(6)	N(4B)–C(15B)	1.321(5)
C(1A)–O(1A)	1.315(5)	C(1B)–O(1B)	1.312(5)
C(15A)–O(2A)	1.303(5)	C(15B)–O(2B)	1.303(5)
N(1A)–Fe(2)–N(5A)	176.68(16)	N(1B)–Fe(1)–N(5B)	175.51(15)
N(1A)–Fe(2)–O(1A)	80.93(13)	N(1B)–Fe(1)–O(1B)	80.97(13)
N(5A)–Fe(2)–O(1A)	96.78(13)	N(5B)–Fe(1)–O(1B)	96.57(13)
N(1A)–Fe(2)–O(2A)	96.76(14)	N(1B)–Fe(1)–O(2B)	95.17(13)
N(5A)–Fe(2)–O(2A)	81.00(14)	N(5B)–Fe(1)–O(2B)	81.28(13)
O(1A)–Fe(2)–O(2A)	95.08(13)	O(1B)–Fe(1)–O(2B)	95.17(12)
N(1A)–Fe(2)–N(6A)	101.45(16)	N(1B)–Fe(1)–N(6B)	102.75(17)
N(5A)–Fe(2)–N(6A)	80.87(15)	N(5B)–Fe(1)–N(6B)	80.90(16)
O(1A)–Fe(2)–N(6A)	89.43(13)	O(1B)–Fe(1)–N(6B)	89.37(13)
O(2A)–Fe(2)–N(6A)	161.71(14)	O(2B)–Fe(1)–N(6B)	162.00(15)
N(1A)–Fe(2)–N(3A)	80.82(16)	N(1B)–Fe(1)–N(3B)	81.26(15)
N(5A)–Fe(2)–N(3A)	101.65(15)	N(5B)–Fe(1)–N(3B)	101.49(15)
O(1A)–Fe(2)–N(3A)	161.09(14)	O(1B)–Fe(1)–N(3B)	161.50(14)
O(2A)–Fe(2)–N(3A)	91.95(14)	O(2B)–Fe(1)–N(3B)	91.50(14)
N(6A)–Fe(2)–N(3A)	89.36(15)	N(6B)–Fe(1)–N(3B)	89.57(15)

A comparison between the X-ray structures of [Fe^{III}(L¹)₂]⁺ and the corresponding free aroylhydrazone ligand (HL¹)^{7a} reveals structural transformations undergone by the Schiff base upon complexation with the ferric ion. The most obvious is the deprotonation of the ligand which occurred along with the structural modification of the amide functional group. In HL¹ the distance of the carbonyl (C=O) bond is 1.219(2) Å,^{7a} but the corresponding carbon–oxygen bonds in [Fe^{III}(L¹)₂]⁺ are considerably longer (with average distances of 1.309 Å in complex cation **A** and 1.308 Å in complex cation **B**), indicative of tautomeric conversion to the enolate C–O⁻ single bond. Simultaneously, the amide N–C single bond [1.347(3) Å] acquires multiple-bond character with the distance shortening to 1.318(5) and 1.321(5) Å in complex cation **B** and 1.337(5) and 1.331(6) Å in complex cation **A**. Complex cation **A** appears to exhibit a greater degree of delocalization of electrons over the ligand backbone on enolisation.

The bond angles in the coordination sphere of **5** (Table 2) define a distorted octahedral geometry at the metal centre. The most linear angle is that of N_{im}–Fe–N_{im}, which is 176.68(16) $^\circ$ for complex cation **B** and 175.51(5) $^\circ$ for complex cation **A**. The other two *trans* angles (N_{py}–Fe–O_{en}) deviate considerably from the idealized angle [complex cation **B**: 162.00(15) $^\circ$ and 161.50(14) $^\circ$; complex cation **A**: 161.71(14) $^\circ$ and 161.09(14) $^\circ$] largely because they are each formed by donor atoms from the *same* highly rigid ligand with an enolate backbone. This coordination behaviour of (L¹)⁻ in [Fe^{III}(L¹)₂]ClO₄ (**5**) mirrors that in the analogous iron(II) complex [Fe^{II}(L¹)₂] (**3**).^{10a} The *cis* angles for complex cation **B** range from 80.90(16) to 101.49(15) $^\circ$ whereas for complex cation **A** they range from 80.82(16) to 101.45(16) $^\circ$. The smallest coordination angles (N_{py}–Fe–N_{im}) are imposed by the five-membered chelate

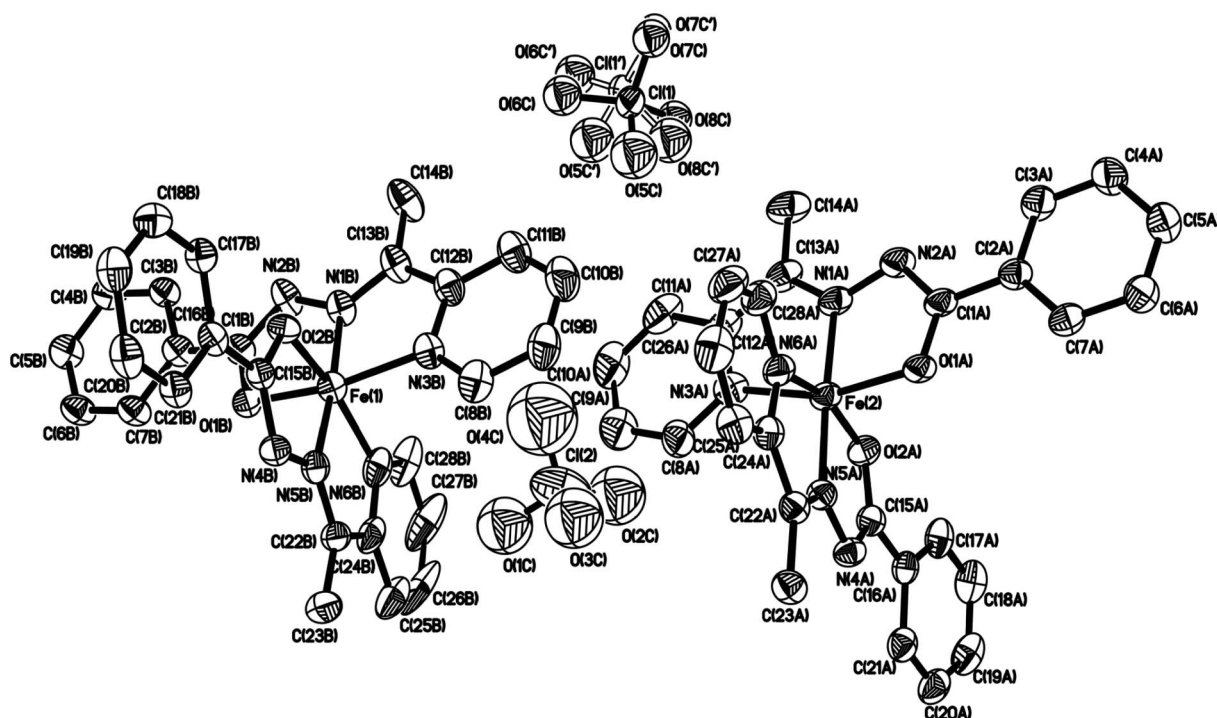


Fig. 1 X-ray structure of $[\text{Fe}^{\text{III}}(\text{L}^1)_2]\text{ClO}_4$ (**5**) at 100 K.

rings and their magnitude in Fe^{III} octahedral geometries is diagnostic of the spin state (HS: $74\text{--}77^\circ$,^{13a,24} LS: $80\text{--}82^\circ$ ^{2d,13a,24b}). Hence these pyridyl-imine bite angles in **5** are consistent with the 2T_2 ground state.

It is now well established that single-crystal X-ray crystallography can distinguish between the spin states of iron(II) or iron(III) in octahedral symmetry. Molecular orbital (MO) theory predicts longer Fe–L bonds in the HS state than in the LS state since the HOMO of the former is antibonding (d_{σ^*}) whereas that of the latter is nonbonding (d_{π}). Indeed every variable-temperature crystallographic study of iron spin crossovers supports this premise. In **5** at 100 K, the average bond distances in the coordination spheres are: Fe– $N_{\text{py}} = 1.948 \text{ \AA}$, Fe– $N_{\text{im}} = 1.879 \text{ \AA}$ and Fe– $O_{\text{en}} = 1.908 \text{ \AA}$ (complex cation **B**) and Fe– $N_{\text{py}} = 1.964 \text{ \AA}$, Fe– $N_{\text{im}} = 1.889 \text{ \AA}$ and Fe– $O_{\text{en}} = 1.902 \text{ \AA}$ (complex cation **A**). These bond distances unequivocally point to the LS state ($S = 1/2$). For $S = 5/2$ (HS), the corresponding distances are markedly longer: Fe– $N_{\text{py}} \sim 2.15\text{--}2.25 \text{ \AA}$,^{13a} Fe– $N_{\text{im}} \sim 2.05\text{--}2.17 \text{ \AA}$ ^{13a} and Fe– $O_{\text{en}} \sim 2.00\text{--}2.08 \text{ \AA}$.⁶ Thus, as a fresh unperturbed crystalline material at 100 K, **5** has a 2T_2 ground state. While the distances of the LS ferric Fe– N_{py} and Fe– N_{im} bonds in **5** are hardly distinguishable from the corresponding ones in the LS ferrous complex **3**,^{10a} the LS ferric Fe– O_{en} bonds are significantly shorter than those of the LS ferrous complex (~ 1.9 vs. $\sim 2.0 \text{ \AA}$). Notably, the Fe– N_{py} and Fe– N_{im} distances closely match those of closely related LS Fe^{III} thiosemicarbazonato complexes.^{24,25}

Magnetic susceptibility measurements of iron aroylhydrazone complexes

The expected oxidation states of iron in these coordination compounds are +2 and +3 with the octahedral spin states LS ($S = 0$) and HS ($S = 2$) belonging to the former and LS ($S = 1/2$) and HS

($S = 5/2$) to the latter. Experimentally, the spin states of iron(II) are recognised by the values of the effective magnetic moment, $\mu_{\text{eff}} = (8\chi_{\text{M}}T)^{1/2}$, commonly observed in the ranges $\sim 5.0\text{--}5.5 \mu_{\text{B}}$ (HS) and $\sim 0.3\text{--}0.9 \mu_{\text{B}}$ (LS).^{12a-d,f,j} On the other hand, the corresponding experimental values for iron(III) are $\sim 5.9 \mu_{\text{B}}$ (HS)^{6a,12e,13,26} and $\sim 1.8\text{--}2.6 \mu_{\text{B}}$ (LT: $\sim 1.8\text{--}2.1 \mu_{\text{B}}$; RT: $\sim 2.0\text{--}2.6 \mu_{\text{B}}$) (LS).^{12e,27} Considering spin-only paramagnetism [$\mu_{\text{S}} = \{2S(S + 1)\}^{1/2}$], all these values of μ_{eff} indicate significant orbital contribution with the exception of HS $\text{Fe}(\text{III})$ which has $L = 0$ in O_{h} symmetry.

The iron compounds **1** (purple-violet), **2** (purple), **4** (dark green), **5** (olive) and **6** (olive) were characterized by magnetic susceptibility measurements. The dark green complex $[\text{Fe}^{\text{II}}(\text{L}^1)_2]$ (**3**) is already known from the literature to be essentially low spin below room temperature and to undergo incomplete spin conversion above room temperature.^{10a} Plots of μ_{eff} vs. T and χ_{M}^{-1} vs. T for the purple-violet compound $[\text{Fe}^{\text{II}}(\text{HL}^1)_2](\text{ClO}_4)_2$ (**1**) are shown in Fig. 2. The former shows normal paramagnetism with a room-temperature value of $\sim 5.15 \mu_{\text{B}}$ indicative of the high-spin state of iron(II) ($t_{2g}^4e_g^2$; $\mu_{\text{S}} = 4.90 \mu_{\text{B}}$) and a modest orbital contribution to the magnetism. Given that $[\text{Fe}^{\text{II}}(\text{L}^1)_2]$ (**3**) is predominantly LS (at RT) and $[\text{Fe}^{\text{II}}(\text{HL}^1)_2](\text{ClO}_4)_2$ (**1**) is HS, it can be deduced that the field strength of the ligand HL^1 is weaker in the keto tautomer than in the enolate form. The same magnetic curve reveals a sharp drop in the values of μ_{eff} from around 20 to 2 K consistent with zero-field splitting.²⁸ The inverse of the molar magnetic susceptibility varies linearly with absolute temperature in accordance with the Curie–Weiss law, $\chi_{\text{M}} = C/(T - \theta)$, giving a value of -2.72 K for the Weiss constant which implies weak antiferromagnetic interactions of the mononuclear paramagnetic centres. Likewise, the other keto complex $[\text{Fe}^{\text{II}}(\text{HL}^2)_2](\text{ClO}_4)_2$ (**2**) is HS with $\mu_{\text{eff}} \sim 5.2 \mu_{\text{B}}$ at RT.

Recently, it has been shown that subtle modifications to the pyridyl aroylhydrazones (such as variations of the nature and position of substituent groups) can bring about dramatic magnetic

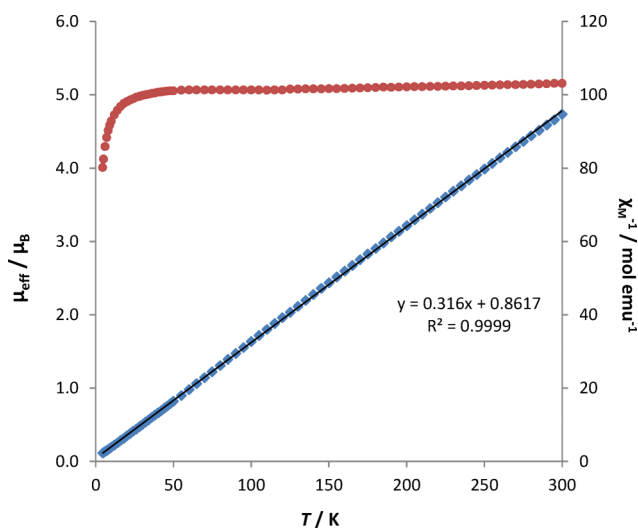


Fig. 2 Temperature dependence of μ_{eff} and χ_{M}^{-1} for $[\text{Fe}^{\text{II}}(\text{HL}^1)_2](\text{ClO}_4)_2 \cdot 2\text{H}_2\text{O}$ (1·2H₂O).

changes. Whereas $[\text{Fe}^{\text{II}}(\text{L}^1)_2]$ is predominantly LS below RT and undergoes an incomplete gradual SCO at elevated temperatures, the complex $[\text{Fe}^{\text{II}}(\text{pcbh})_2]$ (Hpcbh = 2-pyridinecarbaldehyde benzoylhydrazone) has been shown to be HS.^{10a} In contrast, the magnetic moment of the *tert*-butyl-substituted congener of $[\text{Fe}^{\text{II}}(\text{L}^1)_2]$, $[\text{Fe}^{\text{II}}(\text{L}^2)_2]$, lies in the range 0.1–0.9 μ_{B} between 300 and 5 K, consistent with stabilisation of the 1A_1 ground state. Interestingly, the complexes $[\text{Fe}^{\text{II}}(\text{ap2hh})_2]$ (Hap2hh = 2-acetylpyridine 2-hydroxybenzoylhydrazone), $[\text{Fe}^{\text{II}}(\text{pc2hh})_2]$ (Hpc2hh = 2-pyridinecarbaldehyde 2-hydroxybenzoylhydrazone) and $[\text{Fe}^{\text{II}}(\text{pc4hh})_2]$ (Hpc4hh = 2-pyridinecarbaldehyde 4-hydroxybenzoylhydrazone) have been demonstrated to be $^5T_2 \leftrightarrow ^1A_1$ spin crossovers with varying extents of completeness of the spin conversion in the temperature range 2–390 K.¹⁰

The magnetic data of the olive iron(III) compound **5** were collected on a powder formed by grinding large rectangular blocks of the compound. The spin transition curve for **5** reveals complicated magnetic behaviour suggesting gradual multi-step spin conversion (Fig. 3). At 400 K (the limit temperature for the SQUID magnetometer), the compound is predominantly high spin with $\mu_{\text{eff}} \sim 5.5 \mu_{\text{B}}$. The magnetic moment decreases with temperature to a value of $\sim 4.9 \mu_{\text{B}}$ at room temperature. The temperature at which the HS and LS $[\text{Fe}^{\text{III}}(\text{L}^1)_2]^+$ ions exist at equilibrium in equal proportions ($T_{1/2}$) is around 150 K. A quasi-plateau occurs between 100 and 20 K ($\sim 3.5 \mu_{\text{B}}$), after which the magnetic moment drops sharply to $\sim 3.2 \mu_{\text{B}}$ at 5 K. Thus the spin conversion is incomplete at both ends of the magnetic curve.

The value of μ_{eff} at 100 K is somewhat in conflict with the crystallographic analysis of the structure of **5** which implied existence of this iron(III) compound wholly in the low-spin state at that temperature. However, this discrepancy can be attributable to the well-known effects of sample grinding, pulverizing and ball-milling or sample preparation^{13a,29} on spin transitions (see section below on Mössbauer spectroscopy) as well as the influence of solvents of crystallisations^{13b,29c,f,30} on SCO and stabilisation of the spin states of iron. The crystal used for X-ray analysis was solvated while the sample analysed magnetically was not; moreover, the large crystals were crushed for the magnetic measurement.

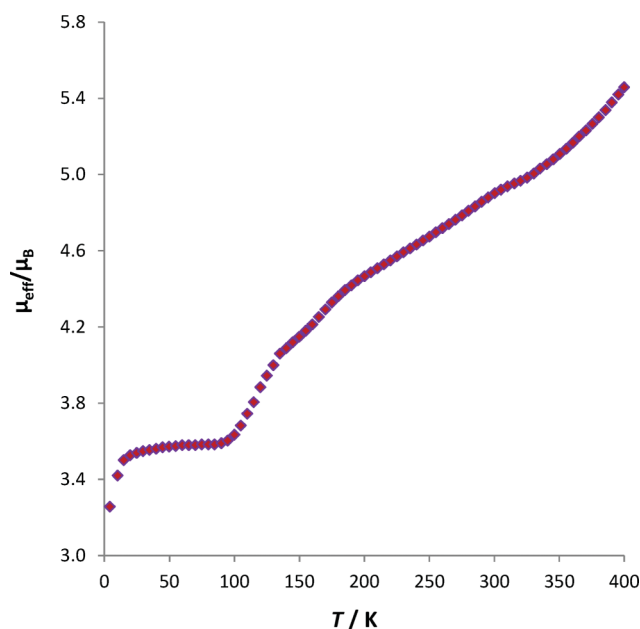


Fig. 3 Temperature dependence of μ_{eff} for $[\text{Fe}^{\text{III}}(\text{L}^1)_2]\text{ClO}_4$ (**5**).

Clearly, the influence of the *tert*-butyl substituent group on the magnetic properties of the iron(III) compounds is evident in Fig. 4. In stark contrast to the magnetic behaviour of $[\text{Fe}^{\text{III}}(\text{L}^1)_2]\text{ClO}_4$ (**5**), $[\text{Fe}^{\text{III}}(\text{L}^2)_2]\text{ClO}_4$ (**6**) exhibits a straightforward gradual spin conversion defined by a sigmoidal $^5T_2 \leftrightarrow ^1A_1$ transition curve with $T_{1/2} \sim 280$ K. The spin crossover is virtually quantitative with $\mu_{\text{eff}} \sim 5.70 \mu_{\text{B}}$ ($\chi_{\text{M}}T = 4.06 \text{ cm}^3 \text{ mol}^{-1} \text{ K}$) at 400 K and $2.00 \mu_{\text{B}}$ ($\chi_{\text{M}}T = 0.500 \text{ cm}^3 \text{ mol}^{-1} \text{ K}$) at 5 K.

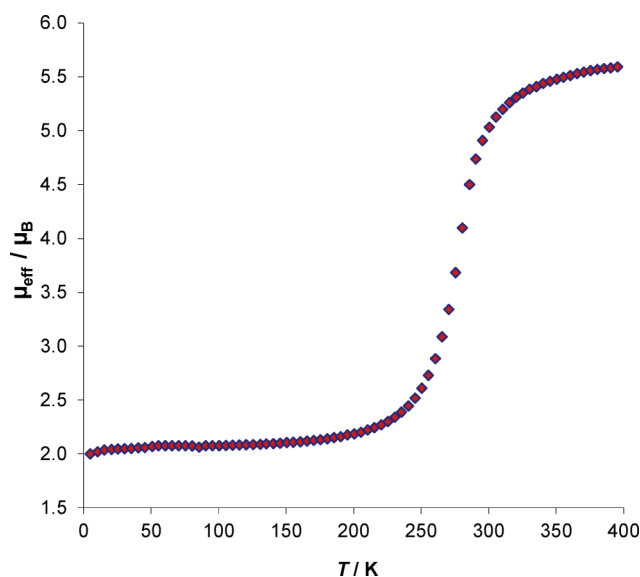


Fig. 4 Temperature dependence of μ_{eff} for $[\text{Fe}^{\text{III}}(\text{L}^2)_2]\text{ClO}_4$ (**6**).

Mössbauer spectroscopy

The spin states of iron(II) and iron(III) are readily distinguishable by their Mössbauer hyperfine parameters. The triply degenerate ground state of each of these iron ions exhibits considerably larger quadrupole splitting (ΔE_{Q}) than does the corresponding

singly degenerate ground state. Apart from a few exceptions, the spin states of iron in six-coordinate complexes have the following parameters:^{12,24a,28a,29h} $\Delta E_Q \sim 2.10\text{--}3.90\text{ mms}^{-1}$, $\delta \sim 0.90\text{--}1.10\text{ mms}^{-1}$ (5T_2 , HS Fe^{II}); $\Delta E_Q \sim 0.20\text{--}1.35\text{ mms}^{-1}$, $\delta \sim 0.30\text{--}0.55\text{ mms}^{-1}$ (1A_1 , LS Fe^{II}); $\Delta E_Q \sim 2.00\text{--}3.20\text{ mms}^{-1}$, $\delta \sim 0.05\text{--}0.25\text{ mms}^{-1}$ (2T_2 , LS Fe^{III}); $\Delta E_Q \sim 0.35\text{--}1.15\text{ mms}^{-1}$, $\delta \sim 0.25\text{--}0.45\text{ mms}^{-1}$ (6A_1 , HS Fe^{III}) (where δ denotes isomer shift).

The Mössbauer spectrum of [Fe^{II}(HL¹)₂](ClO₄)₂·2H₂O (1·2H₂O) (violet crystals) at 295 K displays a high-spin quadrupole-split doublet with $\Delta E_Q = 2.45\text{ mms}^{-1}$ and $\delta \sim 0.99\text{ mms}^{-1}$, consistent with the magnetic moment of this compound at the same temperature. On the other hand, the spectrum of the enolate complex [Fe^{II}(L¹)₂] (**3**) (dark green crystals) at 80 K confirmed the 1A_1 ground state and diamagnetism of this iron(II) compound ($\Delta E_Q = 1.25\text{ mms}^{-1}$, $\delta = 0.29\text{ mms}^{-1}$). The spectrum (Fig. 5) obtained for a freshly prepared, unperturbed microcrystalline sample of **5**·MeOH at 80 K gave an asymmetric, ^{20f,25c,29a,c,h,30b,31} quadrupole-split doublet ($\Delta E_Q = 3.20\text{ mms}^{-1}$, $\delta = 0.11\text{ mms}^{-1}$) consistent with the 2T_2 ground state and in agreement with the low-temperature single-crystal X-ray structure. This result provides incontrovertible evidence that under appropriate conditions the spin transition to $S = 1/2$ does indeed go to completion. Unfortunately, the room-temperature Mössbauer measurement of this compound did not exhibit any absorption.

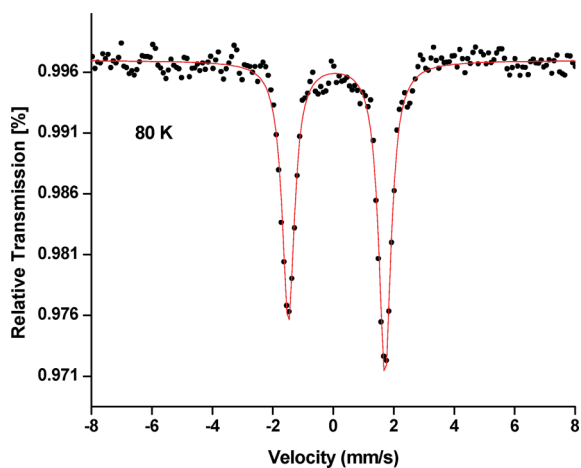
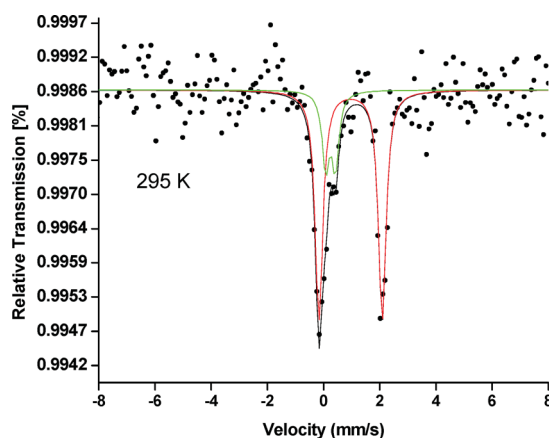
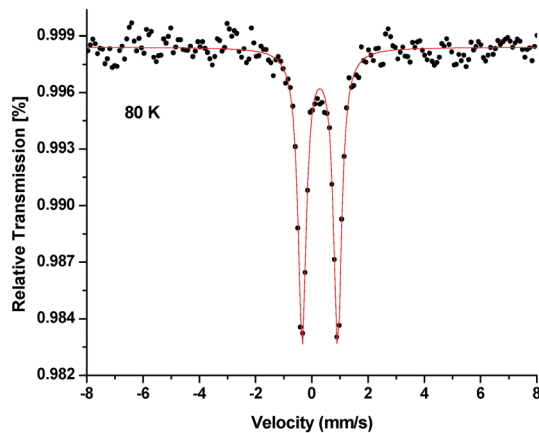


Fig. 5 Mössbauer spectrum of [Fe^{III}(L¹)₂](ClO₄)·MeOH (**5**·MeOH) at 80 K.

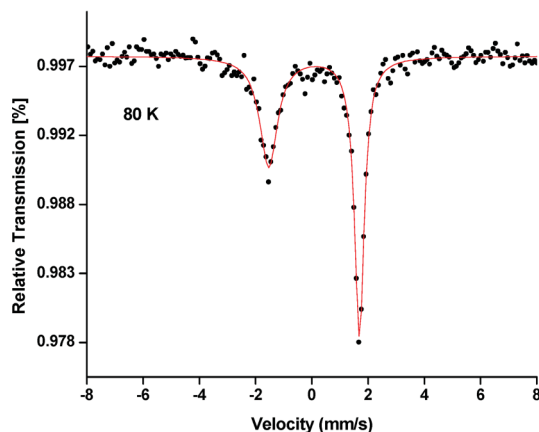
The Mössbauer spectra of the three iron compounds derived from the pyridyl aroylhydrazone HL² are presented in Fig. 6. The spectrum of the keto compound [Fe^{II}(HL²)₂](ClO₄)₂ (**2**) (purple powder) exhibits a doublet with the quadrupole splitting 2.25 mms^{-1} and isomer shift 0.96 mms^{-1} characteristic of a high-spin iron(II) centre. Mössbauer spectroscopy detected an iron(III) ($S = 5/2$) impurity in the sample of **2** by the presence of a very weak quadrupole-split doublet ($\Delta E_Q = 0.35\text{ mms}^{-1}$, $\delta = 0.25\text{ mms}^{-1}$) [Fig. 6(a)]. This is not surprising given that the complex cation [Fe^{II}(HL)₂]²⁺ (Fe²⁺: 2HL) was obtained from a reaction involving equimolar amounts of Fe³⁺: HL. Thus Fe³⁺ was in excess; presumably, some of the unreacted iron(III) from the salt remained in the product powder during isolation and purification. In the case of the other iron(II) molecular compound [Fe^{II}(L²)₂] (**4**) (dark green crystals), the spectrum at 80 K [Fig. 6(b)] gives



(a)



(b)



(c)

Fig. 6 Mössbauer spectra of (a) [Fe^{II}(HL²)₂](ClO₄)₂ (**2**) (295 K), (b) [Fe^{II}(L²)₂] (**4**) (80 K) and (c) [Fe^{III}(L²)₂](ClO₄) (**6**) (80 K).

a symmetric quadrupole-split doublet ($\Delta E_Q = 1.27\text{ mms}^{-1}$, $\delta = 0.29\text{ mms}^{-1}$) indicative of the 1A_1 ground state and corroborating the outcome of the magnetic susceptibility measurement. The spin-crossover compound [Fe^{III}(L²)₂](ClO₄) (**6**) gives rise to a strongly asymmetric, ^{20f,25c,29a,c,h,30b,31} LS (2T_2) quadrupole-split doublet with $\Delta E_Q = 3.22\text{ mms}^{-1}$, $\delta = 0.08\text{ mms}^{-1}$ [Fig. 6(c)] in keeping with the magnetic spin-transition curve (Fig. 4).

The reason for the close match between the magnetic and Mössbauer data is that the samples used were identical (microcrystalline sheets that did not require any grinding) and this compound is non-solvated. As in the case of **5**, there was no Mössbauer absorption observed for **6** at room temperature.

EPR spectroscopy

Conclusive proof of the existence of **5** and **6** in the trivalent state was conveniently provided by EPR spectroscopy; the ferrous state is EPR-inactive. Moreover, the EPR study was crucial to back up the magnetic susceptibility measurements that revealed the occurrence of the ${}^6A_1 \leftrightarrow {}^2T_2$ crossover in these iron(III) compounds, particularly because Mössbauer spectroscopy gave no absorptions at room temperature. The solid-state X-band EPR spectra of **5** and **6** at room and liquid-nitrogen temperatures are exhibited in Fig. 7 and 8, respectively.

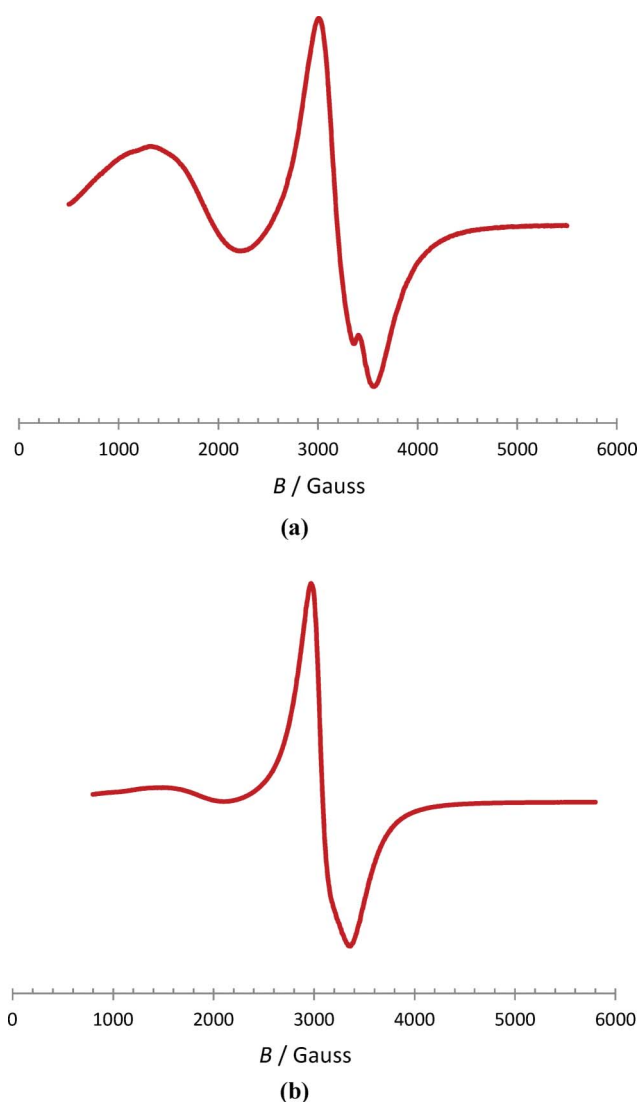


Fig. 7 X-band EPR spectra of $[\text{Fe}^{\text{III}}(\text{L}^1)_2]\text{ClO}_4$ (**5**) at (a) RT and (b) LN temperature.

The RT powder spectrum of **5** comprises a broad HS ($S = 5/2$) resonance centred at $g \sim 5.25$ and axial LS signals at $g =$

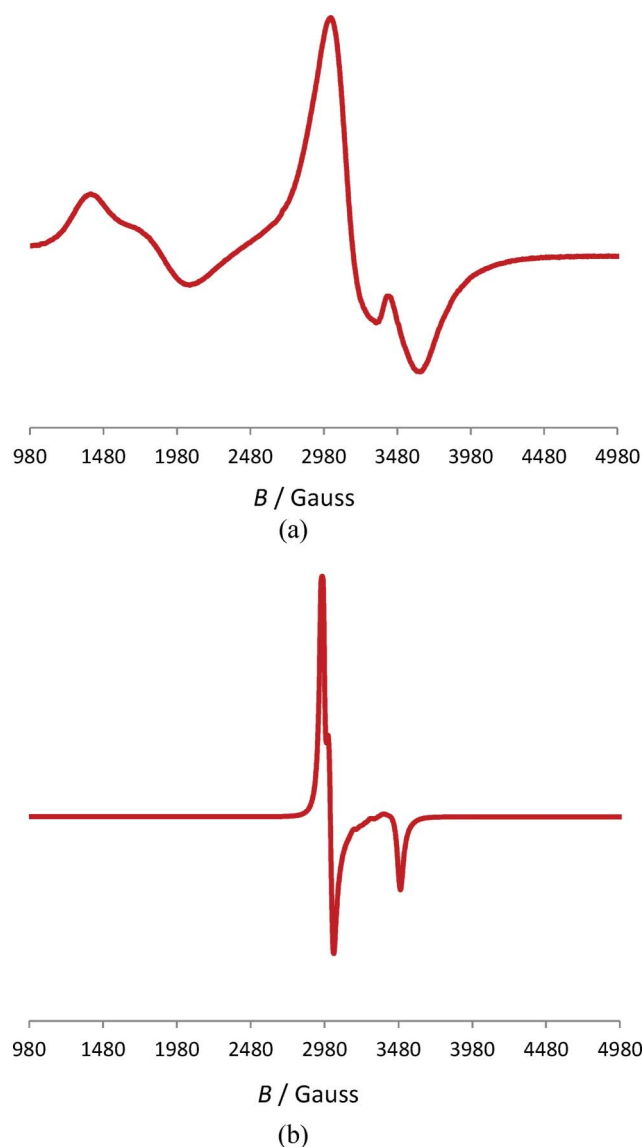


Fig. 8 X-band EPR spectra of $[\text{Fe}^{\text{III}}(\text{L}^2)_2]\text{ClO}_4$ (**6**) at (a) RT and (b) LN temperature.

2.20 and 1.96. On cooling to 77 K, the intensity of the high-spin resonance ($g \sim 4.48$) decreases considerably as this compound becomes predominantly low spin; on the other hand, the low-spin resonance becomes more isotropic ($g \sim 2.19$). The EPR spectra tie in with the magnetic data since the samples used were from the same batch of crystals. The spin-crossover behaviour of the *tert*-butyl-substituted compound **6** differs conspicuously from that of **5** in that it is purely LS at LN temperature (regardless of sample type) as demonstrated by both magnetic susceptibility measurement ($\chi_M T = 0.530 \text{ cm}^3 \text{ K mol}^{-1}$) and EPR spectroscopy [$g_x = 2.28$, $g_y = 2.24$ and $g_z = 1.93$ (LS)]. From the EPR LS rhombic signal, it can be deduced that in LS $[\text{Fe}^{\text{III}}(\text{L}^2)_2]^+$, the unpaired electron resides in a HOMO of d_{xy} character [*i.e.* t_{2g} -configuration = $(d_{yz})^2(d_{xz})^2(d_{xy})^1$ for the Fe^{III} ion].^{1c,d,25a,c,d,32} As expected, at RT $[\text{Fe}^{\text{III}}(\text{L}^2)_2]\text{ClO}_4$ (**6**) shows coexistence of HS and LS complex cations: $g \sim 4.90$ (HS, rhombic), $g_x = g_y = 2.22$ and $g_z = 1.92$ (LS, axial).

X-band EPR spectroscopy has also demonstrated that both compounds **5** and **6** have preference for the doublet ground state

in frozen MeOH solution, as illustrated by the spectrum of **5** in Fig. 9 ($g_x = g_y = 2.23$ and $g_z = 1.93$). Solution chemistry confirms that the keto complex $[\text{Fe}^{\text{II}}(\text{HL})_2](\text{ClO}_4)_2$ ($\text{HL} = \text{HL}^1$ or HL^2) is a precursor of the enolate complexes $[\text{Fe}^{\text{II}}\text{L}_2]$ and $[\text{Fe}^{\text{III}}\text{L}_2]\text{ClO}_4$ (Scheme 3). In MeOH solution, $[\text{Fe}^{\text{II}}(\text{HL})_2](\text{ClO}_4)_2$ converts to $[\text{Fe}^{\text{III}}\text{L}_2]\text{ClO}_4$ instantaneously by aerial oxidation as indicated by the colour change from purple-violet to olive with more definitive evidence obtained from EPR spectroscopy [$g_x = g_y = 2.23$ and $g_z = 1.93$, LS Fe^{III}] (Fig. S4, ESI†).

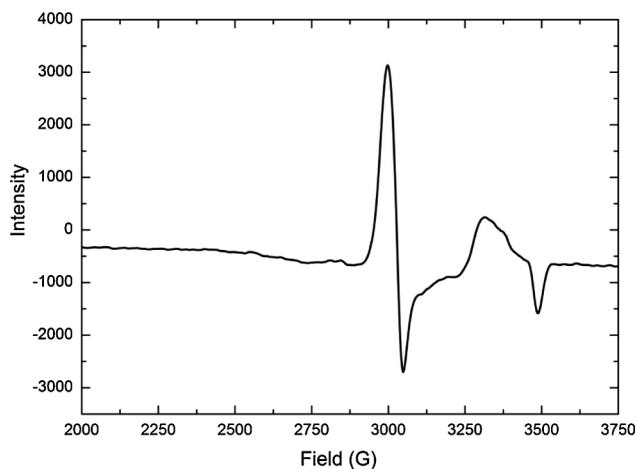
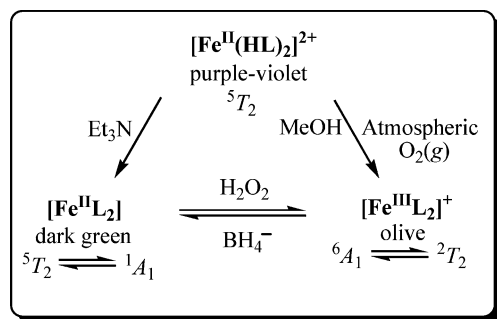


Fig. 9 X-band EPR spectrum of $[\text{Fe}^{\text{III}}(\text{L}^1)_2]\text{ClO}_4$ (**5**) in frozen EtOH/MeOH (5 : 2, v/v) solution at 77 K.



Scheme 3 Conversion of $[\text{Fe}^{\text{II}}(\text{HL})_2]^{2+}$ to $[\text{Fe}^{\text{II}}\text{L}_2]$ and $[\text{Fe}^{\text{III}}\text{L}_2]^+$ in solution.

Addition of Et_3N to $[\text{Fe}^{\text{II}}(\text{HL})_2](\text{ClO}_4)_2$ affords the dark green complex $[\text{Fe}^{\text{II}}\text{L}_2]$ which is not detectable by EPR spectroscopy, but readily identifiable by electronic absorption spectroscopy. Hydrogen peroxide readily oxidises the enolate divalent complex to the corresponding trivalent complex cation.

Electrochemistry

The chemically induced interconversion between $[\text{Fe}^{\text{II}}\text{L}_2]$ and $[\text{Fe}^{\text{III}}\text{L}_2]^+$ illustrated in Scheme 3 demonstrates the ease with which the metal centre shuttles between the divalent and trivalent states as a consequence of the remarkable ability of these pyridyl aroylhydrazones to stabilise both electrovalencies of iron under ambient conditions. Consistent with this solution chemistry, cyclic voltammetry shows that all the iron compounds in this system are redox-active, each exhibiting a totally reversible one-electron redox

process ascribable to the $\text{Fe}^{\text{III}}/\text{Fe}^{\text{II}}$ couple ($E_{1/2} = +0.14$ or 0.15 V vs. SHE in MeCN). An illustrative cyclic voltammetric measurement at various scan rates is given for **6** in Fig. 10.

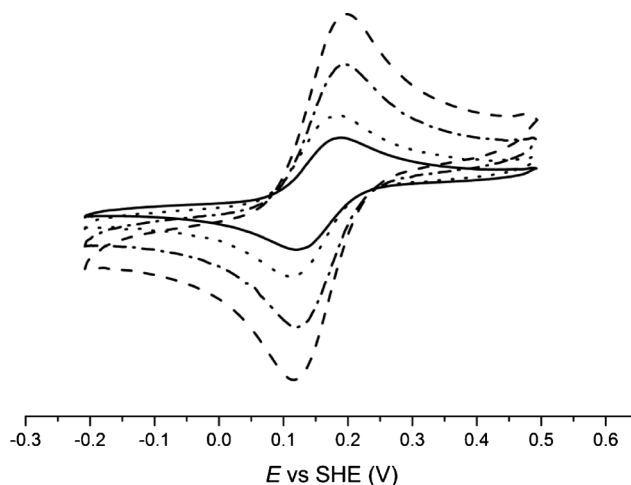


Fig. 10 Cyclic voltammograms of $[\text{Fe}^{\text{III}}(\text{L}^2)_2]\text{ClO}_4$ (**6**) in MeCN at scan speeds of 100, 200, 500 and 1000 mV s^{-1} (from inside outwards).

That the cyclic voltammograms of **5** and **6** are indistinguishable from one another indicates absence of inductive effect of the electron-donating *tert*-butyl substituent group on the redox potential. Interestingly, the values of the $\text{Fe}^{\text{III}}/\text{Fe}^{\text{II}}$ redox potentials for these iron-aroylhydrazone complexes lie within those for the closely related iron complexes with di-2-pyridyl ketone thiosemicarbazones, 2-benzoylpyridine thiosemicarbazones or 2-(3-nitrobenzoyl)pyridine thiosemicarbazones varying from +99 to +249 mV vs. NHE.^{2b-d} These potentials are of particular biological relevance to intracellular oxidants and reductants.

Electronic absorption spectroscopy

The ferrous compounds **1** and **2** are unstable in common solvents such as Me_2CO , MeOH, EtOH, CHCl_3 , CH_2Cl_2 , DMF and DMSO as they undergo spontaneous aerial oxidation to afford the respective ferric compounds **5** and **6** with a colour change from purple to olive. However, $[\text{Fe}^{\text{II}}(\text{HL}^1)_2](\text{ClO}_4)_2$ (**1**) remains intact in MeCN, albeit for a limited period of time. Unfortunately, so far no suitable solvent has been found for the *tert*-butyl-substituted analogue; thus it has not been possible to record the UV-visible spectrum of **2**. On the other hand, the LS iron(II) complexes $[\text{Fe}^{\text{II}}(\text{L}^1)_2]$ (**3**) and $[\text{Fe}^{\text{II}}(\text{L}^2)_2]$ (**4**) and the iron(III) spin-crossover compounds $[\text{Fe}^{\text{III}}(\text{L}^1)_2]\text{ClO}_4$ (**5**) and $[\text{Fe}^{\text{III}}(\text{L}^2)_2]\text{ClO}_4$ (**6**) are soluble and stable in MeOH and a host of other solvents.

The electronic transitions imparting the distinct colours (Fig. 11) to these iron compounds are clearly evident in the representative electronic spectra in Fig. 12. The lopsided broad absorption band (430–630 nm) of the high-spin iron(II) compound **1** (in MeCN), centred at 535 nm ($\epsilon = 1140$ $\text{L mol}^{-1} \text{cm}^{-1}$) [Fig. 12(a)], signifies transference of charge from an iron(II) d_n orbital to an empty low-lying p_π^* orbital of the pyridyl moiety of the aroylhydrazone, giving rise to the strong purple colour of this compound. Unfortunately, the spin-allowed ligand-field (${}^5T_{2g} \rightarrow {}^5E_g$) transition was not observed, although it was previously in the solid state.²¹ It has also been reported for the Fe^{II} complex



Fig. 11 Distinct colours of the iron compounds of HL¹ in solution: [Fe^{II}(HL¹)₂](ClO₄)₂ (**1**) (purple, in MeCN), [Fe^{II}(L¹)₂] (**3**) (green, in MeOH) and [Fe^{III}(L¹)₂]ClO₄ (**5**) (olive, in MeOH).

with 2-[3-(2'-pyridyl)pyrazol-1-ylmethyl]pyridine (HS at RT).³³ Intraligand electronic transitions (predominantly $\pi \rightarrow \pi^*$) occur in the UV region: 260 nm ($\epsilon = 25\,700\text{ L mol}^{-1}\text{ cm}^{-1}$) and 306 nm ($\epsilon = 35\,400\text{ L mol}^{-1}\text{ cm}^{-1}$).

In the case of the LS complexes [Fe^{II}(L¹)₂] (**3**) and [Fe^{II}(L²)₂] (**4**), the dark green colour originates from the Fe^{II} ($d_{\pi} \rightarrow L^{-} (p_{\pi}^*)$) charge-transfer transitions with absorptions at the lower-energy end of the visible spectra. Due to the coordination distortion at the metal centre and possibly $S=2 \leftrightarrow S=0$ interconversion in solution, these MLCT absorption bands are broad and asymmetric. The electronic spectroscopic features of **3** in MeCN have already been reported.^{1f} The UV-visible spectrum of **4**, recorded in MeOH and displayed in Fig. 12(b), shows a maximum visible MLCT absorption at 650 nm ($\epsilon = 2230\text{ L mol}^{-1}\text{ cm}^{-1}$) and ligand-based UV absorptions at 258 nm ($\epsilon = 15\,300\text{ L mol}^{-1}\text{ cm}^{-1}$) and 348 nm ($\epsilon = 21\,800\text{ L mol}^{-1}\text{ cm}^{-1}$). The spin-allowed ligand-field transitions ${}^1A_{1g} \rightarrow {}^1T_{1g}$ and ${}^1A_{1g} \rightarrow {}^1T_{2g}$ ^{12b} were not observed probably because their absorption bands were obscured by the intense CT bands; these LS Fe^{II} d-d absorptions are rarely observed in pyridyl-containing complexes.

The electronic absorption spectra of the iron(III) SCO compounds **5** and **6** are virtually identical and resemble those of the corresponding free ligands but are red-shifted. Their intense olive colour derives from the strong shoulder around 445 nm ($\epsilon \sim 8000\text{ L mol}^{-1}\text{ cm}^{-1}$ for the former and $\sim 8080\text{ L mol}^{-1}\text{ cm}^{-1}$ for the latter) in MeOH [Fig. 12(c)] arising probably from an enolate (O⁻)-to-iron(III) charge-transfer (LMCT) transition. The absence of ligand-field transitions implies existence of these iron(III) compounds completely in the high-spin state in MeOH solution at RT. This contrasts sharply with the EPR measurement at LN temperature which revealed a pure 2T_2 ground state for these compounds. Finally, the ligand-based electronic transitions are evidenced by the following absorption bands: 270 nm ($\epsilon = 33\,000\text{ L mol}^{-1}\text{ cm}^{-1}$) and 355 nm ($\epsilon = 34\,400\text{ L mol}^{-1}\text{ cm}^{-1}$) for **5** and 285 nm ($\epsilon = 28\,700\text{ L mol}^{-1}\text{ cm}^{-1}$) and 353 nm ($\epsilon = 31\,500\text{ L mol}^{-1}\text{ cm}^{-1}$) for **6**.

Concluding remarks

The Schiff-base ligands acetylpyridine benzoylhydrazone (HL¹) and acetylpyridine 4-*tert*-butylbenzoylhydrazone (HL²) were syn-

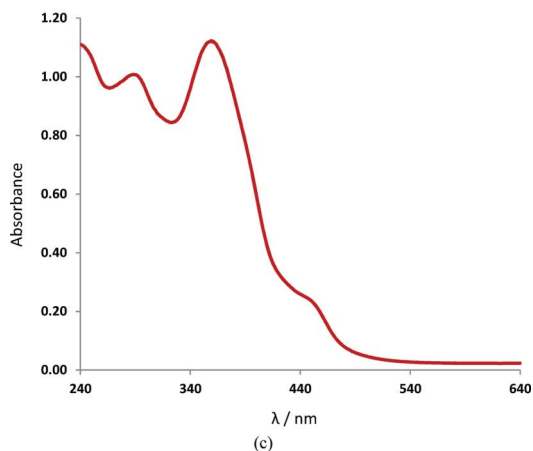
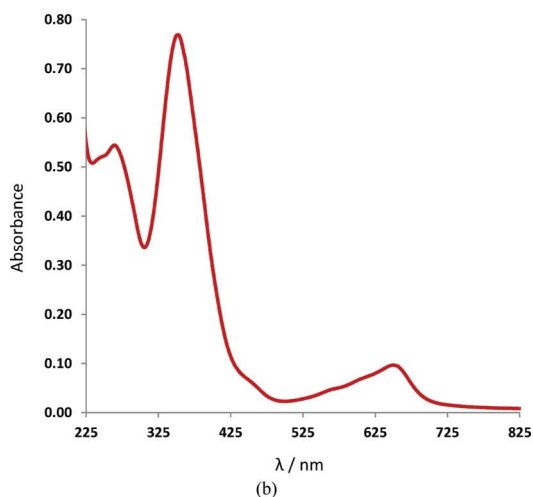
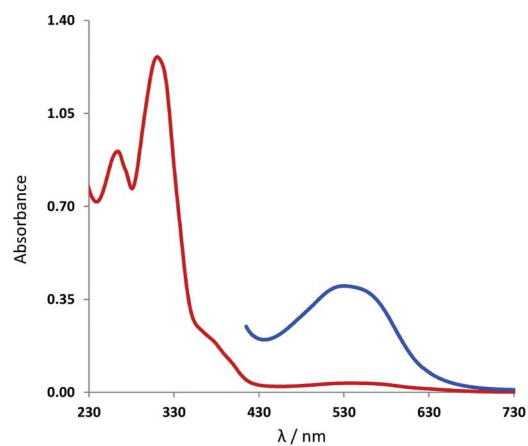


Fig. 12 Electronic absorption spectra of (a) [Fe^{II}(HL¹)₂](ClO₄)₂ (**1**) (0.0350 M, MeCN; inset: 0.350 M, MeCN), (b) [Fe^{II}(L²)₂] (**4**) (0.0350 M, MeOH) and [Fe^{III}(L²)₂]ClO₄ (**5**) (0.0350 M, MeOH).

thesised and isolated in the keto tautomeric form as evidenced by vibrational and NMR spectroscopies. A synthetic strategy exploiting the tendency of aroylhydrazones to readily undergo metal- or base-assisted tautomerisation was used to generate and isolate a set of three visually distinct iron compounds from each of the ligands: high-spin [Fe^{II}(HL¹)₂](ClO₄)₂ (**1** and **2**), low-spin [Fe^{II}L₂] (**3** and **4**) and SCO [Fe^{III}L₂]ClO₄ (**5** and **6**). A bevy of

solid-state and solution experiments and physicochemical measurements have been conducted to ascertain the chemical identities of these compounds and demonstrate the coordination versatility of the pyridyl aroylhydrazones towards iron. The keto compound $[\text{Fe}^{\text{II}}(\text{HL})_2](\text{ClO}_4)_2$ is a precursor of the enolate compounds $[\text{Fe}^{\text{II}}\text{L}_2]$ and $[\text{Fe}^{\text{III}}\text{L}_2]\text{ClO}_4$; interaction with a base tautomerises it to the molecular complex $[\text{Fe}^{\text{II}}\text{L}_2]$ whereas dissolution in MeOH causes spontaneous aerial oxidation to the ionic compound $[\text{Fe}^{\text{III}}\text{L}_2]\text{ClO}_4$. $[\text{Fe}^{\text{II}}\text{L}_2]$ and $[\text{Fe}^{\text{III}}\text{L}_2]^+$ are interconvertible electrochemically. $[\text{Fe}^{\text{III}}(\text{L}^1)_2]\text{ClO}_4$ (**5**) is one of only two known examples of an iron(III) bis-chelate compound with a pyridyl aroylhydrazone to be crystallographically elucidated. Both iron(III) compounds **5** and **6** are the first examples of *ferric* spin-crossover molecular materials derived from *aroylhydrazones*. The spin transition in the former is very sensitive to sample type and solvation. Freshly prepared unperturbed crystalline samples of solvated **5** enable complete ${}^6A_1 \rightarrow {}^2T_2$ conversion at 100 K; the pure LS state at this low temperature has been proven by crystallographic analysis and Mössbauer spectroscopy. In contrast, magnetic susceptibility measurements, EPR spectroscopy and Mössbauer spectroscopy concur that the SCO in the *tert*-butyl-substituted analogue **6** is not affected by sample type and is virtually complete. Electronic absorption spectroscopy suggests that both iron(III) compounds exist in the sextet ground state in MeOH solutions at RT whereas EPR spectroscopy shows preference for the 2T_2 ground state in frozen MeOH solutions at LN temperature. Thus for both iron(III) complexes, the SCO appears to be complete in MeOH solution (300–77 K).

Experimental

Materials and general physicochemical measurements

All chemicals and reagents were commercially obtained in the highest purity possible and were used as received. Whereas 2-acetylpyridine and 4-*tert*-butylbenzoic hydrazide were purchased from Aldrich Chemical Company, benzhydrazide was obtained from ACROS Organics. The salts $\text{Fe}(\text{ClO}_4)_3 \cdot x\text{H}_2\text{O}$ and $\text{Fe}(\text{ClO}_4)_2 \cdot 6\text{H}_2\text{O}$ as well as the solvents MeOH, absolute EtOH and MeCN (each of HPLC or AR grade) were supplied by Aldrich Chemical Company. Et_3N was provided by BDH Chemicals Ltd. (**Warning:** Perchlorate salts are notorious for explosiveness; thus precautionary measures must be taken when handling them. In this work, harmless explosions were experienced during melting point determinations of the iron aroylhydrazone compounds possessing perchlorate as counter anion).

Melting points of the ligands and complexes were determined using a Gallenkamp melting point apparatus. Infrared (IR) spectra were recorded on a Perkin–Elmer Spectrum BX FT-IR spectrophotometer in the range 4000–400 cm^{-1} with the samples compressed as KBr discs using a Carver hydraulic press. ${}^1\text{H-NMR}$ spectra were run on an Avance Bruker 400 MHz spectrometer with CDCl_3 or $\text{DMSO-}d_6$ as solvent and TMS as internal reference standard. Electronic absorption spectra were measured with a Hewlett-Packard 8453 diode-array UV-visible spectrophotometer in the range 190–1100 nm using freshly prepared solutions. Microanalyses were performed on a CE440 CHN elemental analyser. Electron impact (EI) and fast atom bombardment (FAB) mass spectra were recorded on a VG 70-SE mass spectrometer

using 3-nitrobenzyl alcohol as matrix. Conductivity measurements were performed on a Hanna EC215 conductivity meter at room temperature with the molarity of the solutions being 10^{-3} M.

Variable-temperature magnetic susceptibility measurements were carried out on a Quantum Design MPMS-5S SQUID magnetometer with an applied field of 0.8 T. Diamagnetic corrections were made the usual way using Pascal's constants. Mössbauer spectra were measured with a conventional constant-acceleration spectrometer with a 50 mCi ${}^{57}\text{Co}(\text{Rh})$ source of γ -rays and equipped with a low-temperature accessory. The spectrometer was calibrated with α -Fe at RT. X-band electron paramagnetic resonance (EPR) spectra were recorded on a Bruker ELEXSYS E-500 CW spectrometer ($\nu \sim 9.3$ GHz). Cyclic voltammetric measurements were carried out in MeCN on an AUTOLAB/PGSTAT 128 N potentiostat with $[\text{Bu}_4\text{N}]\text{PF}_6$ (0.10 M) as the supporting electrolyte using a three-electrode cell made up of a platinum working electrode, a platinum counter electrode and a AgCl/Ag reference electrode. The redox potentials were calibrated with ferrocene as the internal standard (Fc^+/Fc) and are quoted relative to the standard hydrogen electrode (SHE).

X-ray structure determination

Rectangular-shaped black blocks of $[\text{Fe}^{\text{III}}(\text{apbh})_2]\text{ClO}_4$ (**5**) suitable for single-crystal X-ray analysis were grown from a solution of this compound in MeOH/EtOH (50% v/v) by slow solvent evaporation under ambient conditions over a period of three days. The crystal quality is solvent-dependent; loss of solvent of crystallisation causes failure of X-ray diffraction. X-ray intensity data collection was performed on a Bruker APEX-II CCD area detector diffractometer equipped with graphite-monochromated $\text{Mo-K}\alpha$ radiation ($\lambda = 0.71073$ Å) at 100 K. Absorption correction was performed with the programme *SADABS*.³⁴ The crystal structure was solved by direct methods using *SHELXS-97* and refined with *SHELXL-97* (SHELX suite of programmes).³⁵ All non-hydrogen atoms were refined with anisotropic thermal parameters by full-matrix least-squares calculations based on F^2 . Hydrogen atoms were positioned geometrically and allowed to ride on their respective parent atoms. One of the two perchlorate counter anions [Cl(1), O(5C), O(6C), O(7C), O(8C)] in the crystallographic asymmetric unit is disordered and was refined to an occupancy of 55–45%. A solvent molecule of crystallisation proved difficult to refine, hence the PLATON ‘Squeeze’ function²³ was applied to eliminate it. Pertinent crystallographic data are summarized in Table 1.

Syntheses of aroylhydrazones and corresponding iron complexes

Synthesis of 2-acetylpyridine benzoylhydrazone (HL¹)^{15,10a,21}. A sample of benzhydrazide (2.7233 g, 20.0 mmol) was dissolved in absolute EtOH (100 mL) to give a colourless solution to which 2-acetylpyridine (2.4228 g, 20.0 mmol) was added. The resultant mixture was heated under reflux for 6 h and then kept at room temperature to evaporate slowly and concentrate the solution. After approximately one week, long colourless needles were deposited. These crystals were isolated by decantation, washed with ice-cold ethanol and dried in air at room temperature. Yield: 3.9452 g (82.44%); m.p.: 149–150 °C; Anal. Calcd for $\text{C}_{14}\text{H}_{13}\text{N}_3\text{O}$: C, 70.28; H, 5.48; N, 17.56. Found: C, 70.36; H, 5.41; N, 17.54.

EI-MS: m/z 239. FT-IR (KBr disc): 3176, 3009, 2868, 2864, 1653, 1617 cm^{-1} .

Synthesis of 2-acetylpyridine 4-*tert*-butylbenzoylhydrazone (HL²). To a colourless solution of 4-*tert*-butylbenzoic hydrazide (3.8450 g, 20.0 mmol) in absolute EtOH (100 mL) was added 2-acetylpyridine (2.4228 g, 20.0 mmol). Thereafter, this reaction mixture was heated under reflux for 6 h and then allowed to stand at room temperature for about one fortnight during which time slow evaporation of the solvent afforded a white crystalline solid. This product was washed with ice-cold EtOH and dried in air overnight to give white shiny microcrystals. Yield: 5.4607 g (92.44%); m.p.: 135–137 °C; Anal. Calcd for $\text{C}_{18}\text{H}_{21}\text{N}_3\text{O}$: C, 73.19; H, 7.17; N, 14.23. Found: C, 73.19; H, 7.22; N, 14.20. EI-MS: m/z 295. FT-IR (KBr disc): 3254, 3048, 3014, 2966, 2902, 2868, 1666, 1610 cm^{-1} .

Synthesis of $[\text{Fe}^{\text{II}}(\text{HL}^1)_2](\text{ClO}_4)_2$ (1). 2-Acetylpyridine benzoylhydrazone (0.1922 g, 0.80 mmol) was dissolved in the solvent mixture MeOH/absolute EtOH (40 mL, 50% v/v) by heating under reflux. Then to this solution of the ligand was added iron(II) perchlorate hexahydrate (0.2077 g, 0.80 mmol) and the resultant mixture was heated under reflux for 15 min, giving a dark purple solution. Thereafter, this solution was filtered and left standing at room temperature overnight, whereupon numerous minute purple-violet crystals were formed. This product was filtered off, washed with ice-cold ethanol and dried in air at room temperature. Yield: 0.1841 g (62.77%); m.p.: explosive at 208 °C. Anal. Calcd for $\text{C}_{28}\text{H}_{26}\text{N}_6\text{O}_{10}\text{Cl}_2\text{Fe}$: C, 45.86; H, 3.57; N, 11.46. Found: C, 45.82; H, 3.48; N, 11.35. FAB-MS: m/z 533. FT-IR (KBr disc): 3450, 3064, 2924, 2863, 1605, 1095, 624 cm^{-1} . [N.B.: When the source of the iron(II) was the ferric salt $\text{Fe}(\text{ClO}_4)_3 \cdot x\text{H}_2\text{O}$, the product was solvated: $[\text{Fe}^{\text{II}}(\text{HL}^1)_2](\text{ClO}_4)_2 \cdot 2\text{H}_2\text{O}$. Anal. Calcd for $\text{C}_{28}\text{H}_{30}\text{N}_6\text{O}_{12}\text{Cl}_2\text{Fe}$: C, 43.71; H, 3.93; N, 10.92. Found: C, 43.80; H, 3.67; N, 10.86. EI-MS: m/z 533. FT-IR (KBr disc): 3550, 3448, 3064, 2924, 2863, 1605, 1095, 624 cm^{-1} . This compound was also produced from the HL : M^{III} molar ratio of 2 : 1 under identical reaction conditions. On several occasions the template synthesis was used for convenience.

Synthesis of $[\text{Fe}^{\text{II}}(\text{HL}^2)_2](\text{ClO}_4)_2$ (2). Treatment of a hot solution of 2-acetylpyridine 4-*tert*-butylbenzoylhydrazone (0.2376 g, 0.80 mmol) in a mixture of MeOH and EtOH (40 mL, 50% v/v) with $\text{Fe}(\text{ClO}_4)_3 \cdot x\text{H}_2\text{O}$ (0.2828 g, 0.80 mmol) afforded a reddish purple solution which was heated under reflux for 15 min and filtered. On standing at room temperature for several days, the solution deposited a pale purple solid on the walls of the flask. A suspension of the product was also observed in the solution. This product was filtered off, washed with ice-cold ethanol and dried in air at room temperature. Yield: 0.0570 g (16.85%); m.p.: explosive at 193 °C. Anal. Calcd for $\text{C}_{36}\text{H}_{42}\text{N}_6\text{O}_{10}\text{Cl}_2\text{Fe}$: C, 51.14; H, 5.01; N, 9.94. Found: C, 51.32; H, 5.12; N, 9.87. FAB-MS: m/z 646. FT-IR (KBr disc): 3250, 3092, 2963, 2908, 2868, 1608, 1600, 1130, 1113, 1094, 625 cm^{-1} . [N.B. This iron(II) compound was also obtained from the template reaction of 2-acetylpyridine (0.1211 g, 1.0 mmol), 4-*tert*-butylbenzoic hydrazide (0.1923 g, 1.0 mmol) and $\text{Fe}(\text{ClO}_4)_2 \cdot 6\text{H}_2\text{O}$ (0.1274 g, 0.4 mmol) in refluxing MeOH/EtOH (30 mL, 50% v/v)].

Synthesis of $[\text{Fe}^{\text{II}}(\text{L}^1)_2]$ (3). 2-Acetylpyridine benzoylhydrazone (0.1925 g, 0.80 mmol) was dissolved in a mixture of MeOH

(30 mL) and EtOH (30 mL) to give a colourless solution. Thereafter, Et_3N (0.0810 g, 0.80 mmol) was added to this solution and the resultant reaction mixture was heated under reflux for 15 min, followed by addition of iron(II) perchlorate hexahydrate (0.1026 g, 0.40 mmol) to give a dark green solution instantaneously. This mixture was swirled briefly, heated for 15 min and then filtered. On slow evaporation of the solvent at room temperature over several days, minute shiny black crystals were deposited. This product was isolated by decantation, washed with ice-cold EtOH and dried in air overnight. Yield: 0.0874 g (41.08%); m.p.: 254–255 °C. Anal. Calcd for $\text{C}_{28}\text{H}_{24}\text{N}_6\text{O}_2\text{Fe}$: C, 63.17; H, 4.54; N, 15.79. Found: C, 63.08; H, 4.51; N, 15.82. FAB-MS: m/z 532. FT-IR (KBr disc): 3059, 2969, 2924, 1636, 1594, 1377 cm^{-1} .

Synthesis of $[\text{Fe}^{\text{II}}(\text{L}^2)]$ (4). This iron(II) complex was produced from the reaction of 2-acetylpyridine 4-*tert*-butylbenzoylhydrazone (0.2363 g, 0.80 mmol), Et_3N (0.0810 g, 0.80 mmol) and $\text{Fe}(\text{ClO}_4)_2 \cdot 6\text{H}_2\text{O}$ (0.1019 g, 0.40 mmol) using an analogous synthetic procedure to that described for $[\text{Fe}^{\text{II}}(\text{apbh})_2]$. Shiny black microcrystals were obtained within three days. The product was subsequently isolated from the mother liquor by decantation and then washed with ice-cold ethanol, prior to drying at room temperature. Yield: 0.0786 g (56.26%); m.p.: >400 °C. Anal. Calcd for $\text{C}_{36}\text{H}_{40}\text{N}_6\text{O}_2\text{Fe}$: C, 67.08; H, 6.25; N, 13.04. Found: C, 67.21; H, 6.22; N, 13.13. FAB-MS: m/z 644. FT-IR (KBr disc): 3053, 2962, 2908, 2868, 1609, 1592, 1380 cm^{-1} .

Synthesis of $[\text{Fe}^{\text{III}}(\text{L}^1)_2]\text{ClO}_4 \cdot \text{MeOH}$ (5·MeOH). 2-Acetylpyridine benzoylhydrazone (0.1914 g, 0.80 mmol) was dissolved in a mixture of MeOH and EtOH (60 mL, 50% v/v) to give a colourless solution. Thereafter, Et_3N (0.0810 g, 0.80 mmol) was added with subsequent heating under reflux for 15 min. Treatment of this solution with $\text{Fe}(\text{ClO}_4)_3 \cdot x\text{H}_2\text{O}$ (0.2834 g, 0.80 mmol) caused instantaneous colour change to brown. The resultant reaction mixture was heated under reflux for 15 min and then filtered. Slow evaporation of this solution within one week afforded large black rectangular blocks. These crystals were isolated by decantation, washed with ice-cold EtOH and dried in air overnight. Yield: 0.1542 g (61.02%); m.p.: explosive at 196 °C. Anal. Calcd for $\text{C}_{29}\text{H}_{28}\text{N}_6\text{O}_7\text{ClFe}$: C, 52.47; H, 4.25; N, 12.66. Found: C, 52.22; H, 4.11; N, 12.81. FAB-MS: m/z 532. FT-IR (KBr disc): 3066, 2969, 2919, 1598, 1563, 1359, 1090, 624 cm^{-1} . N.B. From the template reaction of 2-acetylpyridine (0.1211 g, 1.0 mmol), benzhydrazide (0.1362 g, 1.0 mmol) and $\text{Fe}(\text{ClO}_4)_3 \cdot x\text{H}_2\text{O}$ (0.3550 g, 1.0 mmol) in the presence of Et_3N (0.1012 g, 1.0 mmol) the product was isolated as the dihydrate $[\text{Fe}^{\text{III}}(\text{apbh})_2]\text{ClO}_4 \cdot 2\text{H}_2\text{O}$. Anal. Calcd for $\text{C}_{28}\text{H}_{28}\text{N}_6\text{O}_8\text{ClFe}$: C, 50.36; H, 4.23; N, 12.58. Found: C, 50.63; H, 4.13; N, 12.50. The solvents of crystallisation in both $[\text{Fe}^{\text{III}}(\text{L}^1)_2]\text{ClO}_4 \cdot \text{MeOH}$ and $[\text{Fe}^{\text{III}}(\text{L}^1)_2]\text{ClO}_4 \cdot 2\text{H}_2\text{O}$ are lost gradually to form the non-solvated compound $[\text{Fe}^{\text{III}}(\text{L}^1)_2]\text{ClO}_4$. Anal. Calcd for $\text{C}_{28}\text{H}_{24}\text{N}_6\text{O}_6\text{ClFe}$: C, 57.60; H, 4.14; N, 14.39. Found: C, 57.49; H, 4.12; N, 14.31].

Synthesis of $[\text{Fe}^{\text{III}}(\text{L}^2)]\text{ClO}_4$ (6). This iron(III) compound was synthesized by following closely the procedure described for $[\text{Fe}^{\text{III}}(\text{apbh})_2]\text{ClO}_4 \cdot \text{MeOH}$ above using 2-acetylpyridine 4-*tert*-butylbenzoylhydrazone (0.2356 g, 0.80 mmol) as the ligand. The resultant dark brown reaction mixture was allowed to stand at room temperature and slowly evaporate to give a shiny dark olive crystalline material. This product was isolated by decantation and

purified by washing with ice-cold EtOH. After drying in air under ambient conditions, the product appeared as lustrous olive sheets. Yield: 0.1617 g, 47.93%; m.p.: explosive at 213 °C. Anal. Calcd for C₃₆H₄₀N₆O₆ClFe: C, 58.11; H, 5.42; N, 11.30. Found: C, 57.72; H, 5.64; N, 11.09. FAB-MS: *m/z* 644. FT-IR (KBr disc): 3098, 3076, 2964, 2908, 2868, 1602, 1578, 1368, 1108, 1090, 1076, 624 cm⁻¹.

Acknowledgements

Financial support was received with much gratitude from Sultan Qaboos University (M.S.S.: grant # IG/SCI/CHEM/07/02).

Notes and references

- Examples: (a) D. B. Lovejoy and D. R. Richardson, *Blood*, 2002, **100**, 666–676; (b) G. Link, P. Ponka, A. M. Konijn, W. Breuer, Z. I. Cabantchik and C. Hershko, *Blood*, 2003, **101**, 4172–4179; (c) P. V. Bernhardt, L. M. Caldwell, T. B. Chaston, P. Chin and D. R. Richardson, *JBIC, J. Biol. Inorg. Chem.*, 2003, **8**, 866–880; (d) P. V. Bernhardt, P. Chin and D. R. Richardson, *Dalton Trans.*, 2004, 3342–3346; (e) P. V. Bernhardt, P. Chin, P. C. Sharpe and D. R. Richardson, *Dalton Trans.*, 2007, 3232–3244; (f) P. V. Bernhardt, G. J. Wilson, P. C. Sharpe, D. S. Kalinowski and D. R. Richardson, *JBIC, J. Biol. Inorg. Chem.*, 2008, **13**, 107–119.
- Examples: (a) J. Yuan, D. B. Lovejoy and D. R. Richardson, *Blood*, 2004, **104**, 1450–1458; (b) D. R. Richardson, P. C. Sharpe, D. B. Lovejoy, D. Senaratne, D. S. Kalinowski, M. Islam and P. V. Bernhardt, *J. Med. Chem.*, 2006, **49**, 6510–6521; (c) D. S. Kalinowski, Y. Yu, P. C. Sharpe, M. Islam, Y.-T. Liao, D. B. Lovejoy, N. Kumar, P. V. Bernhardt and D. R. Richardson, *J. Med. Chem.*, 2007, **50**, 3716–3729; (d) P. V. Bernhardt, P. C. Sharpe, M. Islam, D. B. Lovejoy, D. S. Kalinowski and D. R. Richardson, *J. Med. Chem.*, 2009, **52**, 407–415.
- D. S. Kalinowski and D. R. Richardson, *Pharmacol. Rev.*, 2005, **57**, 547–583.
- J. M. Donovan, M. Plone, R. Dagher, M. Bree and J. Marquis, *Ann. N. Y. Acad. Sci.*, 2005, **1054**, 492–494.
- (a) A. R. Cohen, *Hematology*, 2006, 42–47; (b) E. Nisbet-Brown, N. F. Olivieri, P. J. Giardina, R. W. Grady, E. J. Neufeld, R. Sechaud, A. J. Krebs-Brown, J. R. Anderson, D. Alberti, K. C. Sizer and D. G. Nathan, *Lancet*, 2003, **361**, 1597–1602.
- Examples: (a) D. Matoga, J. Szklarzewicz, K. Stadnicka and M. S. Shongwe, *Inorg. Chem.*, 2007, **46**, 9042–9044; (b) D. R. Richardson and P. V. Bernhardt, *JBIC, J. Biol. Inorg. Chem.*, 1999, **4**, 266–273; (c) W. Henderson, L. L. Koh, J. D. Ranford, W. T. Robinson, J. O. Svensson, J. J. Vittal, Y. M. Wang and Y. Xu, *J. Chem. Soc., Dalton Trans.*, 1999, 3341–3344.
- Examples: (a) J. Patole, U. Sandbhor, S. Padhye, D. N. Deobagkar, C. E. Anson and A. Powell, *Bioorg. Med. Chem. Lett.*, 2003, **13**, 51–55; (b) C. C. Gatto, E. Schulz, A. Kupfer, A. Hagenbach, D. Wille and U. Abram, *Z. Anorg. Allg. Chem.*, 2004, **630**, 735–741; (c) A. Choudhury, B. Geetha, N. R. Sangeetha, V. Kavita, V. Susila and S. Pal, *J. Coord. Chem.*, 1999, **48**, 87–95; (d) S. Pal, K. R. Radhika and S. Pal, *Z. Anorg. Allg. Chem.*, 2001, **627**, 1631–1637; (e) S. Gao, L.-H. Huo, H. Zhao and S. W. Ng, *Acta Crystallogr., Sect. E: Struct. Rep. Online*, 2005, **E61**, m519–m521; S. Pal and S. Pal, *J. Chem. Soc., Dalton Trans.*, 2002, 2102–2108.
- (a) P. Pelagatti, M. Carcelli, F. Franchi, C. Pelizzi, A. Bacchi, A. Fochi, H.-W. Frühauf, K. Goubitz and K. Vrieze, *Eur. J. Inorg. Chem.*, 2000, 463–475; (b) P. Pelagatti, A. Vergnani, M. Carcelli, M. Costa, D. Rogolino, A. Bacchi and C. Pelizzi, *Inorg. Chim. Acta*, 2003, **351**, 235–241; (c) J. Grewe, A. Hagenbach, B. Stromburg, R. Alberto, E. Vazquez-Lopez and U. Abram, *Z. Anorg. Allg. Chem.*, 2003, **629**, 303–311; (d) S. Nanerjee, A. Ray, S. Sen, S. Mitra, D. L. Hughes, R. J. Butcher, S. R. Batten and D. R. Turner, *Inorg. Chim. Acta*, 2008, **361**, 2692–2700.
- (a) P. V. Bernhardt, P. Chin and D. R. Richardson, *JBIC, J. Biol. Inorg. Chem.*, 2001, **6**, 801–809; (b) P. V. Bernhardt, P. Chin, P. C. Sharpe, J.-Y. C. Wang and D. R. Richardson, *JBIC, J. Biol. Inorg. Chem.*, 2005, **10**, 761–777.
- (a) L. Zhang, G.-C. Xu, H.-B. Xu, V. Mereacre, Z.-M. Wang, A. K. Powell and S. Gao, *Dalton Trans.*, 2010, **39**, 4856–4868; (b) L. Zhang, G.-C. Xu, H.-B. Xu, T. Zhang, Z.-M. Wang, M. Yuan and S. Gao, *Chem. Commun.*, 2010, **46**, 2554–2556.
- J. Tang, J. S. Costa, S. Smulders, G. Molnár, A. Bousseksou, S. J. Teat, Y. Li, G. A. van Albada, P. Gamez and J. Reedijk, *Inorg. Chem.*, 2009, **48**, 2128–2135.
- General overview on spin crossovers: (a) O. Kahn and C. Martinez, *Science*, 1998, **279**, 44–48; (b) P. Gütllich, Y. Garcia and H. A. Goodwin, *Chem. Soc. Rev.*, 2000, **29**, 419–427; (c) J. A. Real, A. B. Gaspar, V. Niel and M. C. Muñoz, *Coord. Chem. Rev.*, 2003, **236**, 121–141; (d) P. Gütllich and H. Goodwin, *Top. Curr. Chem.*, 2004, **233**, 1–47 as well as other articles in this volume; (e) M. Nihei, T. Shiga, Y. Maeda and H. Oshio, *Coord. Chem. Rev.*, 2007, **251**, 2606–2621; (f) M. A. Halcrow, *Polyhedron*, 2007, **26**, 3523–3576; (g) P. Gamez, J. S. Costa, M. Quesada and G. Aromi, *Dalton Trans.*, 2009, 7845–7853; (h) M. Halcrow, *Coord. Chem. Rev.*, 2009, **253**, 2493–2514; (i) B. Weber, *Coord. Chem. Rev.*, 2009, **253**, 2432–2449; (j) J. Olguin and S. Brooker, *Coord. Chem. Rev.*, 2011, **255**, 203–240; (k) J. A. Kitchen, G. N. L. Jameson, J. L. Tallon and S. Brooker, *Chem. Commun.*, 2010, **46**, 3200–3202; (l) D. L. Reger, C. A. Little, M. D. Smith, A. L. Rheingold, K.-C. Lam, T. L. Concolino, G. J. Long, R. P. Hermann and F. Grandjean, *Eur. J. Inorg. Chem.*, 2002, 1190–1197; (m) N. A. Ortega-Villar, M. C. Muñoz and J. A. Real, *Eur. J. Inorg. Chem.*, 2010, 5563–5567.
- Examples: (a) M. S. Shongwe, B. A. Al-Rashdi, H. Adams, M. J. Morris, M. Mikuriya and G. R. Hearne, *Inorg. Chem.*, 2007, **46**, 9558–9568; (b) S. Hayami, Z. Gu, H. Yoshiki, A. Fujishima and O. Sato, *J. Am. Chem. Soc.*, 2001, **123**, 11644–11650; (c) S. Dorbes, L. Valade, J. A. Real and V. Faulmann, *Chem. Commun.*, 2005, 69–71.
- R. J. Butcher, J. R. Ferraro and E. Sinn, *J. Chem. Soc., Chem. Commun.*, 1976, 910–912.
- Examples: (a) W. O. Koch, V. Schünemann, M. Gerdan, A. X. Trautwein and H.-J. Krüger, *Chem.–Eur. J.*, 1998, **4**, 686–691; (b) T. Ikeue, Y. Ohgo, T. Yamaguchi, M. Takahashi, M. Takeda and M. Nakamura, *Angew. Chem., Int. Ed.*, 2001, **40**, 2617–2620; (c) Y. Ohgo, T. Ikeue and M. Nakamura, *Inorg. Chem.*, 2002, **41**, 1698–1700.
- Examples: (a) D. Boinnard, A. Bousseksou, A. Dworkin, J.-M. Savariault, F. Varret and J.-P. Tuchagues, *Inorg. Chem.*, 1994, **33**, 271–281; (b) L. Salmon, A. Bousseksou, B. Donnadieu and J.-P. Tuchagues, *Inorg. Chem.*, 2005, **44**, 1763–1773; (c) B. Weber, W. Bauer and J. Obel, *Angew. Chem., Int. Ed.*, 2008, **47**, 10098–10101; (d) B. Weber, C. Carbonera, C. Desplanches and J.-F. Létard, *Eur. J. Inorg. Chem.*, 2008, 1589–1598.
- (a) Y. Sunatsuki, M. Sakata, S. Matsuzaki, N. Matsumoto and M. Kojima, *Chem. Lett.*, 2001, 1354–1355; (b) Y. Sunatsuki, Y. Ikuta, N. Matsumoto, H. Ohta, M. Kojima, S. Hayami, Y. Maeda, S. Kaizaki, F. Dahan and J.-P. Tuchagues, *Angew. Chem., Int. Ed.*, 2003, **42**, 1614–1618; (c) H. Ohta, Y. Sunatsuki, M. Kojima, S. Iijima, H. Akashi and N. Matsumoto, *Chem. Lett.*, 2004, **33**, 350–351; (d) Y. Sunatsuki, H. Ohta, M. Kojima, Y. Ikuta, Y. Goto, N. Matsumoto, S. Iijima, H. Akashi, S. Kaizaki, F. Dahan and J.-P. Tuchagues, *Inorg. Chem.*, 2004, **43**, 4154–4171; (e) C. Brewer, G. Brewer, R. J. Butcher, E. E. Carpenter, L. Cuenca, B. C. Noll, W. R. Scheidt, C. Viragh, P. Y. Zavalij and D. Zielaski, *Dalton Trans.*, 2006, 1009–1019.
- Examples: (a) B. Li, R.-J. Wei, J. Tao, R.-B. Huang, L.-S. Zheng and Z. Zheng, *J. Am. Chem. Soc.*, 2010, **132**, 1558–1566; (b) J. Klingele, D. Kaase, M. H. Klingele, J. Lach and S. Demeshko, *Dalton Trans.*, 2010, **39**, 1689–1691.
- Example: G. S. Matouzenko, D. Luneau, G. Molnár, N. Ould-Moussa, S. Zein, S. A. Borshch, A. Bousseksou and F. Averseng, *Eur. J. Inorg. Chem.*, 2006, 2671–2682.
- (a) D. Chernyshov, M. Hostettler, K. W. Törnroos and H. B. Bürgi, *Angew. Chem., Int. Ed.*, 2003, **42**, 3825–3830; (b) M. Hostettler, K. W. Törnroos, D. Chernyshov, B. Vangdal and H. B. Bürgi, *Angew. Chem., Int. Ed.*, 2004, **43**, 4589–4594; (c) K. W. Törnroos, M. Hostettler, D. Chernyshov, B. Vangdal and H. B. Bürgi, *Chem.–Eur. J.*, 2006, **12**, 6207–6215; (d) S. Bonnet, M. A. Siegler, J. S. Costa, G. Molnár, A. Bousseksou, A. L. Spek, P. Gamez and J. Reedijk, *Chem. Commun.*, 2008, 5619–5621; (e) N. Bréfuel, H. Watanabe, L. Toupet, J. Come, N. Matsumoto, E. Collet, K. Tanaka and J.-P. Tuchagues, *Angew. Chem., Int. Ed.*, 2009, **48**, 9304–9307; (f) M. Griffin, S. Shakespeare, H. J. Shepherd, C. J. Harding, J.-F. Létard, C. Desplanches, A. E. Goeta, J. A. K. Howard, A. K. Powell, V. Mereacre, Y. Garcia, A. D. Naik, H. Müller-Bunz and G. G. Morgan, *Angew. Chem., Int. Ed.*, 2011, **50**, 896–900.
- S. E. Livingstone and J. E. Oluka, *Transition Met. Chem.*, 1978, **3**, 261–267.

- 22 W. J. Geary, *Coord. Chem. Rev.*, 1971, **7**, 81–122.
- 23 (a) A. L. Spek, *Acta Crystallogr., Sect. A*, 1990, **46**, C40; (b) A. L. Spek, *PLATON, A Multipurpose Crystallographic Tool*, Utrecht University, Utrecht, The Netherlands, 1998; (c) A. L. Spek, *J. Appl. Crystallogr.*, 2003, **36**, 7–13.
- 24 (a) S. Hayami, Z. Gu, M. Shiro, Y. Einaga, A. Fujishima and O. Sato, *J. Am. Chem. Soc.*, 2000, **122**, 7126–7127; (b) G. Juhász, S. Hayami, O. Sato and Y. Maeda, *Chem. Phys. Lett.*, 2002, **364**, 164–170.
- 25 Examples: (a) J. Garcia-Tojal, J. L. Pizarro, L. Lezama, M. I. Arriortua and T. Rojo, *Inorg. Chim. Acta*, 1998, **278**, 150–158; (b) D. X. West, J. K. Swearingen, J. Valdés-Martínez, S. Hernández-Ortega, A. K. El-Sawaf, F. van Meurs, A. Castiñeiras, I. Garcia and E. Bermejo, *Polyhedron*, 1999, **18**, 2919–2929; (c) A. Sreekanth and M. R. P. Kurup, *Polyhedron*, 2004, **23**, 969–978; (d) A. Sreekanth, H.-K. Fun and M. R. P. Kurup, *J. Mol. Struct.*, 2005, **737**, 61–67.
- 26 M. S. Shongwe, C. H. Kaschula, M. S. Adsetts, E. W. Ainscough, A. M. Brodie and M. J. Morris, *Inorg. Chem.*, 2005, **44**, 3070–3079.
- 27 N. Arulsamy and D. J. Hodgson, *Inorg. Chem.*, 1994, **33**, 4531–4536.
- 28 (a) G. Lemercier, E. Mulliez, C. Brouca-Cabarrecq, F. Dahan and J.-P. Tuchagues, *Inorg. Chem.*, 2004, **43**, 2105–2113; (b) I. S. Jahro, D. Onggo, Ismunandar, S. I. Rahayu, M. C. Muñoz, A. B. Gaspar, M. Seredyuk, P. Gütllich and J. A. Real, *Inorg. Chim. Acta*, 2008, **361**, 4047–4054.
- 29 Examples: (a) M. S. Haddad, W. D. Federer, M. W. Lynch and D. N. Hendrickson, *Inorg. Chem.*, 1981, **20**, 131–139; (b) E. W. Müller, H. Spiering and P. Gütllich, *Chem. Phys. Lett.*, 1982, **93**, 567–571; (c) M. D. Timken, D. N. Hendrickson and E. Sinn, *Inorg. Chem.*, 1985, **24**, 3947–3955; (d) A. F. Stassen, E. Dova, J. Ensling, H. Schenk, P. Gütllich, J. G. Haasnoot and J. Reedijk, *Inorg. Chim. Acta*, 2002, **335**, 61–68; (e) D. J. Rudd, C. R. Goldsmith, A. P. Cole, D. N. Stack, K. O. Hodgson and B. Hedman, *Inorg. Chem.*, 2005, **44**, 1221–1229; (f) B. Weber, E. S. Kaps, C. Desplanches and J.-F. Létard, *Eur. J. Inorg. Chem.*, 2008, 2963–2966; (g) C. A. Kilner and M. A. Halcrow, *Dalton Trans.*, 2010, **39**, 9008–9012; (h) H. Oshio, K. Kitazaki, J. Mishiko, N. Kato, Y. Maeda and Y. Takashima, *J. Chem. Soc., Dalton Trans.*, 1987, 1341–1347.
- 30 Examples: (a) A. P. Summerton, A. A. Diamantis and M. R. Snow, *Inorg. Chim. Acta*, 1978, **27**, 123–128; (b) A. J. Conti, R. K. Chadha, K. M. Sena, A. L. Rheingold and D. N. Hendrickson, *Inorg. Chem.*, 1993, **32**, 2670–2680; (c) B. A. Leita, S. M. Neville, G. J. Halder, B. Moubaraki, C. J. Kepert, J.-F. Létard and K. S. Murray, *Inorg. Chem.*, 2007, **46**, 8784–8795; (d) J. C. Dias, B. Vieira, I. C. Santos, L. C. J. Pereira and V. da Gama, *Inorg. Chim. Acta*, 2009, **362**, 2076–2079; (e) W. Bauer, W. Scherer, S. Altmannshofer and B. Weber, *Eur. J. Inorg. Chem.*, 2011, 2803–2818.
- 31 Examples: (a) R. H. Petty, E. V. Dose, M. F. Tweedle and L. J. Wilson, *Inorg. Chem.*, 1978, **17**, 1064–1071; (b) M. S. Haddad, M. W. Lynch, W. D. Federer and D. N. Hendrickson, *Inorg. Chem.*, 1981, **20**, 123–131; (c) Y. Maeda, N. Tsutsumi and Y. Takashima, *Inorg. Chem.*, 1984, **23**, 2440–2447; (d) Y. Maeda, H. Oshio, Y. Takashima, M. Mikuriya and M. Hidaka, *Inorg. Chem.*, 1986, **25**, 2958–2962; (e) M. Mohan, N. Gupta, L. Chandra, N. K. Jha and R. S. Prasad, *Inorg. Chim. Acta*, 1988, **141**, 185–192; (f) S. Hayami, S. Miyazaki, M. Yamamoto, K. Hiki, N. Motokawa, A. Shuto, K. Inoue, T. Shinmyozu and Y. Maeda, *Bull. Chem. Soc. Jpn.*, 2006, **79**, 442–450.
- 32 (a) J. C. Noveron, M. M. Olmstead and P. K. Mascharak, *Inorg. Chem.*, 1998, **37**, 1138–1139; (b) J. M. Rowland, M. Olmstead and P. K. Mascharak, *Inorg. Chem.*, 2001, **40**, 2810–2817; (c) A. K. Patra, M. M. Olmstead and P. K. Mascharak, *Inorg. Chem.*, 2002, **41**, 5403–5409.
- 33 S. Singh, V. Mishra, J. Mukherjee, N. Seethalekshmi and R. Mukherjee, *Dalton Trans.*, 2003, 3392–3397.
- 34 G. M. Sheldrick, *SADABS: A programme for absorption correction with the Siemens SMART system*, University of Göttingen, Germany, 1996.
- 35 G. M. Sheldrick, *Acta Crystallogr., Sect. A: Found. Crystallogr.*, 2008, **64**, 112–122.